KUOPION YLIOPISTON JULKAISUJA C. LUONNONTIETEET JA YMPÄRISTÖTIETEET 197
KUOPIO UNIVERSITY PUBLICATIONS C. NATURAL AND ENVIRONMENTAL SCIENCES 197

MIKKO HAKULINEN

Prediction of Density, Structure and Mechanical Properties of Trabecular Bone Using Ultrasound and X-ray Techniques

Doctoral dissertation

To be presented by permission of the Faculty of Natural and Environmental Sciences of the University of Kuopio for public examination in Auditorium L3, Canthia building, University of Kuopio, on Friday 16th June 2006, at 12 noon

Department of Physics, University of Kuopio
Department of Anatomy, University of Kuopio
Department of Clinical Physiology and Nuclear Medicine, Kuopio University Hospital

KUOPION YLIOPISTO
KUOPIO 2006

Distributor:
Kuopio University Library
P.O. Box 1627
FI-70211 KUOPIO
FINLAND
Tel. +358 17 163 430
Fax +358 17 163 410
http://www.uku.fi/kirjasto/julkaisutoiminta/julkmyyn.html

Series Editors:
Professor Pertti Pasanen, Ph.D.
Department of Environmental Sciences

Professor Jari Kaipio, Ph.D.
Department of Applied Physics

Author´s address:
Department of Physics
University of Kuopio
P.O. Box 1627
FI-70211 KUOPIO
FINLAND
Tel. +358 17 162 342
Fax +358 17 163 032
E-mail: mikko.hakulinen@uku.fi

Supervisors:
Professor Jukka Jurvelin, Ph.D.
Department of Physics
University of Kuopio

Docent Juha Töyräs, Ph.D.
Department of Clinical Neurophysiology
Kuopio University Hospital

Professor Heikki Kröger, M.D., Ph.D.
Department of Surgery
Kuopio University Hospital

Reviewers:
Dr. Christian Langton, Ph.D.
Centre of Metabolic Bone Disease
Hull Royal Infirmary, UK

Docent Harri Sievänen, Sc.D.
Bone Research Group
UKK Institute, Tampere

Opponent:
Dr. Patrick H.F. Nicholson, Ph.D.
Department of Health Science
University of Jyväskylä

ISBN 951-27-0355-6
ISBN 951-27-0450-1 (PDF)
ISSN 1235-0486

Kopijyvä
Kuopio 2006
Finland

Hakulinen, Mikko. Prediction of density, structure and mechanical properties of trabecular bone using ultrasound and X-ray techniques. Kuopio University Publications C. Natural and Environmental Sciences 197. 2006. 84 p.
ISBN 951-27-0355-6
ISBN 951-27-0450-1 (PDF)
ISSN 1235-0486

ABSTRACT

A significant bone loss, typically in combination with a deterioration in bone architecture, is called osteoporosis. Millions of people are affected by this metabolic disease and suffer from osteoporotic fractures. The current clinical method for diagnosis of osteoporosis is the dual energy X-ray absorptiometry (DXA). Quantitative ultrasound (QUS), which is an inexpensive, portable and non-ionizing technique, has been introduced as an alternative method for use in osteoporosis diagnostics.

In this study, bovine and human trabecular bone was investigated by using a wide range of ultrasound frequencies. Further, the microstructure of the human trabecular bone was characterized with a high resolution computed tomography (microCT) technique. Both bovine and human bone samples were tested mechanically to reveal the relationships between the acoustic and mechanical properties of the trabecular bone. The effect of frequency on the ability of ultrasound technique to predict density, structural and mechanical properties of human trabecular bone was evaluated. In addition, artefacts in the DXA technique arising from the variations in the soft tissue and bone marrow composition were numerically evaluated. Additionally, a dual energy X-ray laser (DXL) technique was assessed and compared *in vivo* with DXA.

The experiments and numerical analyses revealed potential errors in DXA measurements related to non-uniform soft tissue composition. The results suggested that the DXL technique may improve the accuracy of bone density measurements, in comparison to the traditional DXA technique. Acoustic measurements revealed that scattering parameters, integrated reflection coefficient (IRC) and broadband ultrasound backscatter (BUB), as well as speed of sound (SOS) were significant predictors of the density and the mechanical properties of human trabecular bone. It was revealed that the sensitivity of QUS parameters to changes in human trabecular bone density, mechanical and structural properties was dependent on the ultrasound frequency.

To conclude, scattering parameters, derived from the pulse-echo ultrasound measurements, may have clinical significance in the diagnostics of osteoporosis. Although 0.5 MHz is the most widely used ultrasound frequency in clinical QUS applications, the present results, conducted with different ultrasound center frequencies suggest that higher frequencies (2.25 MHz-5 MHz) could provide substantial information on the microstructure and mechanical properties of trabecular bone that cannot be obtained at lower frequencies. Based on the knowledge gained in the present study, novel ultrasound techniques that utilize backscatter measurements and higher frequencies are under further testing.

Universal Decimal Classification: 534-8, 534.6, 534.7
National Library of Medicine Classification: QT 34, QT 36, WE 200, WE 250, WN 208
Medical Subject Headings: bone and bones/ultrasonography; ultrasonics; osteoporosis/diagnosis; biomechanics; acoustics; bone density; densitometry, X-ray; numerical analysis, computer-assisted; models, theoretical

To Hanna, Anton and Aaron

ACKNOWLEDGMENTS

This study was carried out in the Departments of Physics and Anatomy, University of Kuopio and Department of Clinical Physiology and Nuclear Medicine, Kuopio University Hospital during the years 2002-2006. I would like to express my deepest gratitude to all persons who have contributed to this study and provided their valuable support throughout the work. I wish to mention the following persons and funding sources.

First of all, I would like thank my principal supervisor Professor Jukka Jurvelin, Ph.D., for his professional and dynamic guidance. I am very grateful for the opportunity to work in his enthusiastic group.

I express my sincere gratitude to my other supervisor, Docent Juha Töyräs, Ph.D., for his intensive and intellectual supervision. It has been my privilege to work with a talented senior researcher who is so unconditionally devoted to science.

I would also like to thank my supervisor Professor Heikki Kröger, M.D., Ph.D., for his guidance and knowledge concerning bone and osteoporosis

I am deeply indebted to Professor Heikki Helminen, M.D., Ph.D., for placing the resources of the Department of Anatomy at my disposal during the thesis work. I am very thankful to him for his fatherly attitude, supervision and wisdom that he has shared.

I want to express my sincere thanks to Professor Harrie Weinans, Ph.D., and Dr. Judd Day, Ph.D., for their professional guidance and continuous support concerning the microCT- measurements. I am grateful for the opportunity to be able to work in the Erasmus MC, Department of Orthopaedics in Rotterdam.

I express much thanks to our Biophysics of Bone and Cartilage (BBC) research group including following persons: Rami Korhonen, Ph.D., Mikko Laasanen, Ph.D., Miika Nieminen Ph.D., Petro Julkunen, M.Sc. (Eng.), Mikko Nissi, physics student, Heikki Nieminen, physics student, Eveliina Lammentausta, M.Sc., Jatta Kurkijärvi, M.Sc., Jarno Rieppo, B.M. and Ossi Riekkinen, M.Sc. The atmosphere in our group has been inspirational and supportive throughout these years. I send my special thanks to my co-author Simo Saarakkala, M.Sc., for the companionship and invaluable cooperation from the very beginning of this thesis. I am very grateful to Jani Hirvonen, M.Sc. (Eng.) and Matti Timonen, B.Sc., for their support in software programming.

I want to express my deepest gratitude to reviewers, Docent Harri Sievänen, Sc.D. and Dr. Christian Langton, Ph.D., for their constructive criticism and advice that helped to improve this thesis. I am grateful to Ewen MacDonald, Ph.D., for linguistic revision.

I send many thanks to Atria Oyj, and their personnel for providing fresh bone material for our *in vitro* studies.

I am greatly indebted to my mother and sister, Tuija and Mia Hakulinen, for

their whole-hearted support and encouragement, for their invigorating attitude and atmosphere during these years.

Finally, I want to express my utmost and dearest thanks to my beloved wife Hanna for her continuous support, unconditional love and understanding during this project, and to our darling sons Anton and Aaron. Their presence has made this thesis possible.

The study was financially supported by the Finnish Biomaterial Graduate School, Finnish Graduate School in Musculoskeletal Diseases, the National Technology Agency (TEKES), Kuopio University Hospital (EVO grant 5173), Instrumentarium Science Foundation, East Finland High Technology Foundation, the Academy of Finland, which I acknowlegde with gratitude.

Kuopio, June 2006

Mikko Hakulinen

SYMBOLS

A	amplitude
a	radius
c	sound speed
$\bar{c}$	velocity
d	diameter
E	(elastic) Young's modulus
f	frequency
Δf	frequency range
F	force
G	shear modulus
h	height
H	area-averaged mean curvature
I	intensity
K	gaussian curvature
K_a	adiabatic bulk modulus
L	length after deformation
L_0	original length
M	mass
max	maximum
min	minimum
n	number of samples
N	X-ray photon count
p	statistical significance
$\underline{p}$	structure point
R	reflection coefficient
r	Pearson's correlation coefficient
s	thickness
T	transmission coefficient
t	time
Δt	time difference
u	particle displacement amplitude
u_0	maximum particle displacement
v	particle velocity
$\mathbf{w}$	two dimensional vector of displacement of the medium
Z	characteristic impedance
x	distance
$\underline{x}$	center of sphere
α	attenuation coefficient
β_0	number of bone particles
β_1	connectivity

β_2	number of cavities
χ	Euler number
ϵ	strain
ϵ_y	yield strain
ϵ_0	zero strain
η	shear viscosity
Δ	Laplace operator
γ	first Lame constant
δ	second Lame constant
κ	principal curvature
θ	angle
τ	local thickness
μ_b	backscatter coefficient
ν	Poisson's ratio
Ω	volume structure
Φ	bulk viscosity
ρ	material density
σ	stress
σ_{max}	ultimate strength
σ_y	yield stress

ABBREVIATIONS

AA	average attenuation
AP	anterior-posterior
AVU	apparent velocity of ultrasound
BMC	bone mineral content
BMD	bone mineral density
BMI	body mass index
BUA	broadband ultrasound attenuation
BUB	broadband ultrasound backscatter
BS	bone surface
BS/BV	bone surface-to-volume ratio
BV	bone volume
BV/TV	bone volume fraction
CC	cephalo-caudal
CT	computed tomography
CV	coefficient of variation
DA	degree of anisotropy
DXA	dual energy X-ray absorptiometry
FC	femoral caput

FE	finite element
FFT	fast Fourier transform
FG	femoral groove
FLC	femoral lateral condyle
FMC	femoral medial condyle
FTM	femoral trochanter major
IRC	integrated reflection coefficient
MIL	mean intercept length
ML	medial-lateral
MRI	magnetic resonance imaging
nBUA	normalized broadband ultrasound attenuation
OR	odds ratio
OSI	osteo sono-assessment index
PBS	phosphate buffered saline
PE	pulse-echo
PD	proximal-distal
pDXA	peripheral dual energy X-ray absorptiometry
pQCT	peripheral quantitative computed tomography
ROI	region of interest
RR	risk ratio
sCV	standardized coefficient of variation
SD	standard deviation
SI	superior-inferior
SMI	structural model index
SOS	speed of sound
SPA	single photon absorptiometry
STP	standard temperature (273.15 K) and pressure (101.325 kPa)
Tb.Sp.	trabecular spacing
Tb.Th.	trabecular thickness
TMP	tibial medial plateau
TOF	time of flight
TT	through-transmission
TV	tissue volume
UTV	ultrasound transmission velocity
vBMD	volumetric bone mineral density
VOS	velocity of sound
QCT	quantitative computed tomography
QUI	quantitative ultrasound index
QUS	quantitative ultrasound
WHO	World Health Organization

LIST OF ORIGINAL PUBLICATIONS

This thesis is based on the following original articles, which are referred to in the text by their Roman numerals (I-IV):

I Hakulinen MA, Saarakkala S, Töyräs J, Kröger H, Jurvelin JS. Dual energy X-ray laser measurement of calcaneal bone mineral density.
Physics in Medicine and Biology 48: 1741-1752, 2003.

II Hakulinen MA, Töyräs J, Saarakkala S, Hirvonen J, Kröger H, Jurvelin JS. Ability of ultrasound backscattering to predict mechanical properties of bovine trabecular bone.
Ultrasound in Medicine and Biology 30: 919-927, 2004.

III Hakulinen MA, Day JS, Töyräs J, Timonen M, Kröger H, Weinans H, Kiviranta I, Jurvelin JS. Prediction of density and mechanical properties of human trabecular bone *in vitro* by using ultrasound transmission and backscattering measurements at 0.2-6.7 MHz frequency range.
Physics in Medicine and Biology 50: 1629-1642, 2005.

IV Hakulinen MA, Day JS, Töyräs J, Weinans H, Jurvelin JS. Ultrasonic characterization of human trabecular bone microstructure.
Physics in Medicine and Biology 51: 1633-1648, 2006.

Contents

Chapter I

Introduction

Bone, which is one of the hardest tissues in the body, adapts to changes in physical loading through a continual process of structural remodeling (Wolff's law) [175]. Osteoporosis is regarded as a metabolic disease in which the dynamic balance between bone resorption and formation is impaired [42]. The first sign of osteoporosis is a gradual reduction of bone mass, which leads to deterioration in bone structure and increased susceptibility to fractures. Several methods have been developed for the assessment of bone quality; single photon absorptiometry (SPA), dual energy X-ray absorptiometry (DXA), single X-ray absorptiometry (SXA), peripheral quantitative computed tomography (pQCT), magnetic resonance imaging (MRI), X-ray absorptiometry and quantitative ultrasound (QUS) techniques have been applied clinically. According to the World Health Organization (WHO) criterion [177], osteoporosis is diagnosed when the BMD value is 2.5 standard deviations or more below the mean for healthy, young adults. Currently, osteoporosis diagnosis is generally based on the bone mineral density (BMD) measurement assessed with the dual energy X-ray absorptiometry (DXA) technique. However, susceptibility to bone fracture is related not only to amount of bone, but also to tissue structure and organic composition [123, 164, 131, 3, 125]. Therefore, DXA can provide only partial information about bone status. Clinical techniques capable of revealing information on bone structure and composition, in addition to the amount of bone mineral, would be clinically useful.

Since the 1980s, when quantitative ultrasound was first introduced as an alternative technique for osteoporosis diagnosis, it has been studied extensively. However, the precision and accuracy of clinical QUS measurements have not been as good as those for DXA. Generally, the instruments are incapable of measuring properties of potential fracture sites, *e.g.* proximal femur, lumbar spine or wrist [114]. Variations in the composition of soft tissue and bone marrow as well as in bone size, diminish reliability of both DXA and clinical QUS techniques [13, 12, 153, 152, 106, 178]. Therefore, interest has become focused on an alternative QUS technique, *i.e.* backscatter

measurements [134, 166, 179]. In principle, backscatter measurements may be conducted from typical fracture sites, *e.g.* proximal femur, that cannot be accessed by using the current clinical QUS technique based on through-transmission measurements. Previous studies have demonstrated the feasibility of using backscatter measurements in the assessment of bone status [23, 63, 171, 134].

In this study, the relationships between acoustic, mechanical and structural properties of trabecular bone were investigated experimentally and numerically. Experimental *in vitro* tests were conducted using bovine and human trabecular bone samples. Multiple ultrasound frequencies were used in the acoustic measurements. The main aim was to find the most sensitive frequency for the assessment of the mechanical and structural characteristics of trabecular bone. In addition, the sources of error in DXA measurement were explored and the performance of new dual energy X-ray laser (DXL) technique for the assessment of bone density was validated both experimentally *in vivo* and by using numerical analyses.

CHAPTER II

Trabecular bone structure and mechanical properties

2.1 Structure and composition of trabecular bone

Bone tissue consists of cells, fibers and ground substance, and in that way it resembles other connective tissues, but unlike the others, its extracellular components are calcified. This characteristic feature of bone makes it a strong, stiff material ideally suited for undertaking locomotive, supportive and protective functions in the skeleton. It provides a framework for the attachment of muscles and tendons that are essential for the locomotion. In addition to these mechanical functions, bone acts as a reservoir for several minerals, for example it stores about 99% of the body's calcium supplies [42]. Bone exhibits a fascinating ability to grow, adapt and repair itself, enabling it to function throughout the lifespan. Bone can be found in different forms varying from dense and compact bone (cortical bone) to spongy, porous type of bone (trabecular bone) (Figure 2.1). Osteoporosis affects an estimated 75 million people in USA, Europe and Japan. It is considered as a metabolic disease in which trabecular bone remodeling is impaired. This metabolic malfunction leads to a gradual reduction of bone mass and a deterioration of bone structure (Table 2.1).

Three kinds of cells are identified in constantly renewing bones: *osteoblasts*, *osteocytes* and *osteoclasts*. Osteoblasts are responsible for the formation of osseous tissue and are constantly found on the advancing surfaces of developing or growing bones. When these cells are surrounded with the matrix, they become quiescent and are known as osteocytes. Osteoclasts, multinucleated giant cells, are responsible for bone resorption and remodeling [9]. Bone remodeling is a consequence of the balanced combination of new bone deposition and mineralization by active osteoblasts and the selective resorption of formed bone by osteoclasts [146].

The bone matrix contains organic and inorganic constituents. **The organic** phase represents approximately 35% of the dry weight of the bone matrix. Collagen fibers, mainly type I, make up 80% - 90% of the organic component. Type I collagen is a fibrillar protein formed from three protein chains, wound together in

a triple helix. Type I collagen is highly cross-linked by covalent bonds. In addition to collagen, the organic phase contains proteoglycan molecules with short protein cores to which the glycosaminoglycans are covalently bound [42].

Table 2.1: Densities [14, 66] and structural [65, 66, 92] characteristics of healthy and osteoporotic trabecular bone in different skeletal locations.

	BMD (g/cm^2)	BV/TV (%)	Tb.Th. (μm)	Tb.Sp. (μm)	SMI (-)	DA (-)
Vertebrae						
Healthy	1.04	14	268	957	2.51	1.15
Osteoporotic	0.79	10	238	1111	2.65	1.43
Radius						
Healthy	0.37	46	240	280	-	-
Osteoporotic	0.19	37	200	350	-	-
Calcaneus						
Healthy	0.83	32	600	1380	-	-
Osteoporotic	0.70	23	540	1840	-	-

BMD = bone mineral density, BV/TV = bone volume fraction, Tb.Th. = trabecular thickness, Tb.Sp. = trabecular spacing, SMI = structural model index and DA = degree of anisotropy.

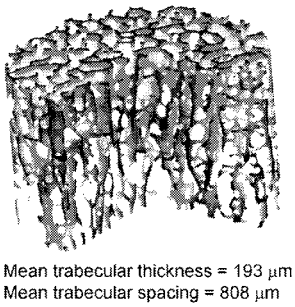

Figure 2.1: A high resolution computed tomography image of a cylindrical (d = 8mm) human trabecular bone sample. Trabecular bone consists of delicate bars and sheets of bone *i.e.* trabeculae, which branch and intersect to form a sponge-like network. The trabecular network orientates along the principal loading direction. The ends of long bones, pelvis and spine consist mainly of trabecular bone.

The inorganic phase represents about 65% of the dry weight of the bone matrix. The inorganic phase consists mainly of calcium and phosphorus, and only small amounts of bicarbonate, magnesium, citrate, sodium and potassium are present [42]. Calcium and phosphorus form hydroxyapatite crystals ($Ca_{10}(PO_4)_6(OH)_2$) and amorphous calcium phosphate. The apatite crystals and collagen fibers create a structure which effectively resists mechanical stresses [9].

2.2 Mechanical properties of trabecular bone

Although bone densitometry is often used for the assessment of bone fragility, mechanical testing only provides direct information about mechanical integrity. From the mechanical point of view, trabecular bone is a highly anisotropic and heterogeneous visco-elastic material. A number of methods, such as compressive, bending or torsion testing, have been developed to permit the quantitative evaluation of the mechanical properties of trabecular bone. The relationship between the applied load and the corresponding deformation is characterized by the stress-strain curve. The stress-strain curve for bone can be divided into *elastic* and *plastic* regions. Within the elastic region, the deformation imitates the movement of a spring. The deformation increases linearly with the increasing load, and after the load is released the bone returns to its original shape. The slope of the stress-strain curve within the elastic region, called the elastic or *Young's modulus* (E), represents the intrinsic stiffness of the sample [156]. The point where the elastic deformation ends and the plastic deformation begins is called the *yield point* (Figure 2.2).

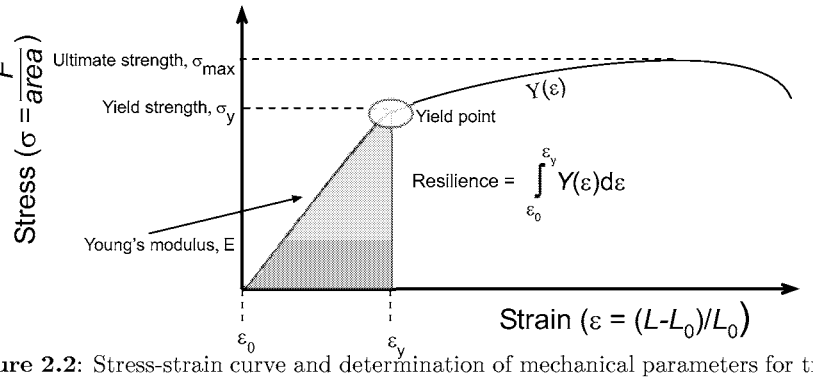

Figure 2.2: Stress-strain curve and determination of mechanical parameters for trabecular bone. Ultimate strength, σ_{max}, is determined as a maximum stress detected during the test. Yield point is defined by the point where the elastic deformation ends and the plastic deformation starts. Yield stress (σ_y) and yield strain (ϵ_y) are the stress and strain values recorded at the yield point. Resilience is defined as the energy stored during elastic deformation. Young's (elastic) modulus, E, is determined as a slope of the linear part of the stress-strain curve. ϵ_0 is the zero strain, F is the applied force, L_0 is the original length of the sample and L is the length of the sample after the deformation.

The *yield strength* (σ_y) and *yield strain* (ϵ_y) are defined by the stress and strain at the yield point, respectively. Resilience represents the amount of energy stored within the elastic region of the stress-strain curve and it is calculated by integrating the stress-strain curve from zero strain (ϵ_0) to yield strain (Figure 2.2). Beyond the yield point, the external stress produces permanent damage to the bone structure. This permanent deformation is called plastic deformation and the region beyond the

yield point is defined as the plastic region of the stress-strain curve. The maximum stress that a bone can sustain is called *ultimate strength* (σ_{max}). Table 2.2 summarizes mechanical properties of trabecular bone of different species in various skeletal sites and loading directions.

Table 2.2: Mechanical properties (mean ± SD) of trabecular bone.

Author	Parameter	Orientation	Site
Human			
Nicholson *et al* [111]	E = 164±72 MPa	SI	Vertebrae
	E = 52±31 MPa	AP	
	E = 43±25 MPa	ML	
Wachter *et al* [163]	E = 52±44 MPa	45° osteotomy	Proximal femur
	σ_{max} = 1.1±1.0 MPa	of a femoral neck	
Giesen *et al* [43]	E = 373±197 MPa	SI, ML	Mandibular condyles
	σ_{max} = 3.3±2.0 MPa		
Langton *et al* [87]	E = 36±23 MPa	ML	Calcaneus
	σ_{max} = 0.5±0.3 MPa		
Dog			
Ding *et al* [29]	E = 1514 (1313-1715) MPa	CC	Vertebrae
	E = 549 (445-653) MPa	ML	
	E = 436 (337-537) MPa	AP	
	σ_{max} = 15.5 (13.4-17.6) MPa	CC	
Bovine			
Töyräs *et al* [158]	σ_{max} = 11.1±3.3 MPa	ML	FMC
	σ_{max} = 7.0±2.8 MPa	ML	FLC
	σ_{max} = 16.1±4.3 MPa	ML	FC
Njeh *et al* [117]	E = 1195±617 MPa	PD	Proximal and
	E = 770±453 MPa	AP	distal femur
	E = 931±496 MPa	ML	
Drozdzowska *et al.* [33]	E = 737±440 MPa	PD	Distal radius
	E = 398±264 MPa	AP	
	σ_{max} = 25.5±4.4 MPa	PD	
	σ_{max} = 11.9±3.7 MPa	AP	

SI, superior-inferior; CC, cephalo-caudal; PD, proximal-distal; AP, anterior-posterior; ML, medial-lateral; FMC, femoral medial condyle; FLC, femoral lateral condyle; FC, femoral caput

In some cases, **compressive tests** may be less accurate than **tensile tests** due to the end artefacts, such as misalignment of the sample with the platens used for loading the sample during the test. On the other hand, compressive tests have advantages as they do not require samples as large as the tensile test, this being

a major advantage in the case of trabecular bone. In addition, preparation of the samples for the compressive test is not as difficult as with the tensile test. In most cases, both tensile and compressive tests serve as precise measurements of bone mechanical properties [156]. In the case of small animals (*e.g.* rodents), the sample preparation for the compressive or tensile test is challenging.

Since trabecular bone is a heterogeneous material, it exhibits a wide variation in mechanical properties. This heterogeneity results from the variations in bone volume fraction, architecture and tissue properties. Elastic modulus and strength of trabecular bone vary both within and across skeletal sites [17, 48, 81, 101]. Although these properties clearly depend on density, the roles of microarchitecture and composition remain partially unclear. Several studies [60] with both human and bovine trabecular bone have shown that up to 94% of the variations in the elastic modulus can be explained with the combination of volume fraction, trabecular orientation and anisotropy. In addition, the changes in microstructure, loss of connectivity and removal of trabeculae can significantly decrease bone strength in osteoporosis [123]. Although the changes in architectural properties such as trabecular number and trabecular thickness are strongly related to the bone density, the effects of these properties on the tissue mechanical integrity are quite different. The bone modulus and strength are more sensitive to the reduction of the trabecular number than to a uniform reduction in trabecular thickness even though this may cause the same loss of bone volume and the same decrease in density [141]. In addition, it has been demonstrated that the toughness and strength of bone are significantly decreased after artificial collagen damage [165]. Several studies have demonstrated that the organic composition of trabecular bone changes in osteoporosis [3, 83, 144, 26] and perhaps these changes may be associated with an increased risk of fractures.

CHAPTER III

Quantitative ultrasound techniques

3.1 Basic physics of ultrasound

Ultrasound consists of propagating mechanical oscillations with a frequency (>20kHz) exceeding the hearing range. A longitudinal waves are generally used in medical ultrasound applications. The longitudinal wave can propagate through all types of media, gases, fluids and solids. In addition to the longitudinal wave, several other progressing waves, *e.g.* transverse, surface and plane waves, exist.

Although energy is transmitted through the medium due to the wave motion, the net movement of the medium is not required for this to occur. The particle displacement amplitude u depends on the distance x along the direction of propagation of the wave. In general terms

$$u = u_0 \sin\left(\omega\left[t - \frac{x}{\bar{c}}\right]\right) \tag{3.1}$$

where $\bar{c}$ is the propagation velocity of the wave, u_0 is the maximum displacement amplitude and $\left(\omega\left[t - \frac{x}{\bar{c}}\right]\right)$ is the phase angle of the wave. $\omega = 2\pi f$, where f is the frequency of the wave. The transmission of the wave, and thereby the sound speed (c) is related to the density and elasticity of the medium (Table 3.1). In the case of longitudinal waves in isotropic solids, the shear rigidity of the medium couples some of the longitudinal wave to the transverse wave [176]. Therefore, the sound speed depends on both bulk and the shear modulus (Table 3.1). The wave velocity ($\bar{c}$), defined in equation (3.1), is called the *phase velocity* and represents the velocity at which any fixed phase of the cycle is displaced. The phenomenon in which velocity of ultrasound is related to the frequency of the wave is called *sound dispersion*, but in biological materials, ultrasound velocity exhibits only a small dispersion. When the medium is dispersive, the velocity is called the *group velocity* which represents the energy propagation velocity. The group velocity has a physical meaning (velocity of energy) only for dispersive medium. For a pulsed

wave in a dispersive medium, group velocity is the velocity of the wave packet [115]. For most practical applications in medicine, the ultrasound velocity is independent of frequency. Sound speed in several organic and inorganic materials is listed in Table 3.2. The *characteristic impedance* (Z) of a material is defined as a product of density (ρ) and sound speed (c) of the medium (Table 3.1).

Table 3.1: Basic ultrasound equations.

Parameter	Equation
Sound speed in fluids [176]	$c = \sqrt{\frac{K_a}{\rho}}$
Sound speed in isotropic solids [176]	$c = \sqrt{\frac{K_a + \frac{4}{3}G}{\rho}}$
	$c = \sqrt{\frac{E(1-\nu)}{(1-2\nu)(1+\nu)\rho}}$
Sound pressure (for the plane waves)	$p = \rho c v$
Characteristic impedance	$Z = \rho c$
Snell's law for refraction	$\frac{\sin\theta_i}{\sin\theta_t} = \frac{c_2}{c_1}$
Reflection coefficient [174]	$R = \left(\frac{Z_2\cos\theta_1 - Z_1\cos\theta_2}{Z_2\cos\theta_1 + Z_1\cos\theta_2}\right)^2$
Transmission coefficient [174]	$T = \frac{4Z_1Z_2\cos\theta_1\cos\theta_2}{(Z_2\cos\theta_1 + Z_1\cos\theta_2)^2}$
Ultrasound Intensity	$I = I_0 e^{-2\alpha(f)x}$

c = sound speed, K_a = adiabatic bulk modulus, G = shear modulus, E = Young's modulus, ν = Poisson's ratio, Z = characteristic impedance, R = reflection coefficient, T = transmission coefficient, α = attenuation coefficient, I = intensity of the wave, v = particle velocity, x = distance and ρ = mean density of the medium, respectively. θ_1 and θ_2 are the angles of the incidence and refraction, respectively. Subscripts 1 and 2 refer to the first and second medium.

When the ultrasound wave meets the boundary of two different media, it may be partially reflected. Analogously to optics, the reflection follows geometrical laws (Table 3.1). Ultrasound scattering results from the interaction between the ultrasound wave and medium particles, *i.e.* acoustic inhomogeneities within the medium. As a result, a secondary (scattered) ultrasound wave is emitted. The scattering depends on the dimension of the scatterers relative to the wavelength of the ultrasound wave. In a case of *Rayleigh scattering*, the scatterers are much smaller than the wavelength and the scattering coefficient is inversely proportional to fourth power of the wavelength. With scatterers comparable in size with the wavelength, the scattered wave exhibits a complex distribution, which is strongly governed by the scatterer dimensions and the acoustic impedance [174, 35].

As the ultrasound wave travels through a medium, it becomes attenuated due to absorption, reflection and scattering. In a reflected and scattered ultrasound wave, energy no longer moves in the original direction, attenuating the primary ultrasound wave. Absorption mechanisms involve energy conversion, typically to heat. Detailed descriptions of absorption mechanisms can be found in the literature [174].

Table 3.2: Acoustic properties of organic [80, 115, 174, 173] and inorganic [40, 47, 99, 150, 159, 174, 78] materials. * Temperatures are within the range 17°C to 25°C, ** Temperatures are within the range 20°C to 37°C.

Material*	**Speed of Sound** (m/s)	**Characteristic Impedance** ($kg/m^2s \times 10^6$)
Air at STP	330	0.0004
Water	1480	1.5
Polyethylene	2000	1.8
Lead	1200	14
Mercury	1450	20
Aluminium	6400	18
Brass, mean	4490	38
Tissue**		
Fat	1450	1.38
Brain	1541	1.58
Blood	1570	1.61
Kidney	1561	1.62
Human tissue, mean	1540	1.63
Spleen	1566	1.64
Liver	1549	1.65
Muscle	1550-1630	1.65-1.74
Articular cartilage	1630	1.71
Skull bone	4080	7.80
Cortical bone	3000-4000	4-8
Trabecular bone	1450-1800	-

3.2 Clinical QUS techniques in osteoporosis diagnostics

At the moment, clinical QUS devices are typically based on the *through-transmission* technique (Figure 3.1). In a through-transmission measurement, the ultrasound transducers are situated at both sides of the object. When ultrasound propagates through medium, *e.g.* bone, the velocity of transmission and the propagation amplitude are influenced by the medium properties. Thus, bone tissue may be characterized by measuring the ultrasound velocity and attenuation. In terms of ultrasound velocity, no established terminology or calculation protocol exists. Speed of sound (SOS, Table 3.3), velocity of sound (VOS), apparent speed of sound, apparent velocity of ultrasound (AVU) and ultrasound transmission velocity (UTV) refer to same ultrasound measurement principle. Several techniques for the detection of pulse transit time exist. These methods include earliest detectable deviation from zero [50], detection of zero-crossing points [15], application of cross-correlation technique [25], predetermined amplitude point or threshold detection [19] and phase spectral analysis [136, 107]. Nicholson *et al* [107] demonstrated significant differences in

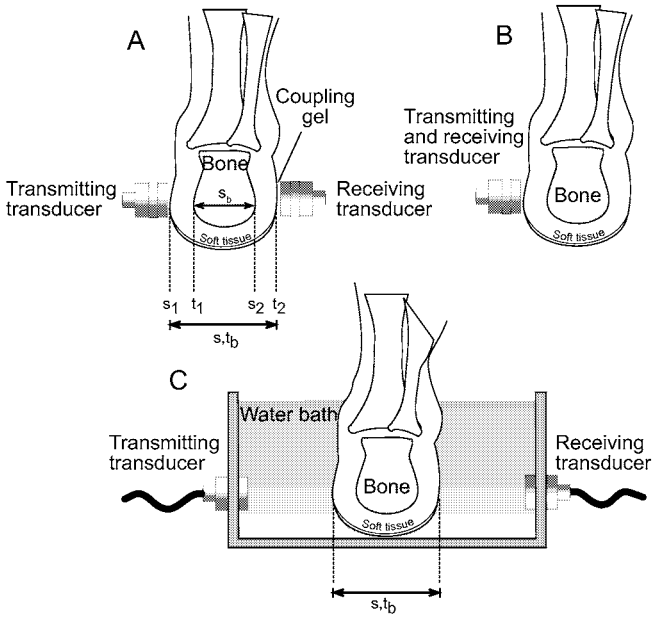

Figure 3.1: Quantitative ultrasound measurement techniques. A) Through-transmission: contact method; B) pulse-echo method; C) through-transmission: substitution method. s_1, s_2 and t_1, t_2 are the thicknesses of the soft tissue and the transit times through them, respectively. s is the heel thickness, s_b is the thickness of the calcaneus and t_b is the transit time through the heel.

magnitude and precision of velocity values when different transit time determination methods were used. In present clinical devices, a variety of the above-mentioned methods are used [115]. In contrast, ultrasound attenuation is defined similarly in most commercial devices, *i.e.* by determining the broadband ultrasound attenuation (BUA, Table 3.3). First, the attenuation is determined as a function of frequency by dividing the amplitude spectrum measured through a reference media (typically degassed water) with the spectrum obtained through the sample [88]. Further, BUA is determined as a slope of the linear part of the attenuation spectrum, in commercial devices usually between 0.2 MHz and 0.6 MHz. Several manufacturers have derived other parameters based on combinations of BUA and velocity. *Stiffness index* (Achilles+, Lunar, Madison, WI, USA), *quantitative ultrasound index* (QUI) (Sahara, Hologic Inc., Bedford, MA, USA) and *osteo sono-assessment index* (OSI) (AOS-100, Aloka, Tokyo, Japan) have been introduced. It has been suggested that both BUA and SOS can identify patients who are at an increased risk of osteoporosis as reliably as BMD [4, 53]. However, some limitations are associated with current clinical QUS techniques. Both BUA and SOS depend on the bone size [157, 88] and, over a wide range of bone densities, BUA has been demonstrated to exhibit a nonlinear association with BMD [62, 138, 158].

Table 3.3: Definitions for basic ultrasound parameters used in clinical applications.

Parameter	Equation
Speed of Sound	$\frac{c_w s}{s-(\Delta t c_w)}$
Bone Velocity	$\frac{s_b}{t_b} = \frac{t-(s_1+s_2)}{t_b-(t_1+t_2)}$
Limb Velocity	$\frac{s}{t_s}$
Broadband Ultrasound Attenuation [88]	$8.686\ln \frac{A_w(f)}{A_b(f)} + \ln(T_{tb}T_{bt})$
Average Attenuation	$\frac{\int_{\Delta f} \alpha_{dB} df}{\Delta f}$
Integrated Reflection Coefficient [27]	$\frac{\int_{\Delta f} (R_b(f))_{dB} df}{\Delta f}$
Broadband Ultrasound Backscatter [134]	$\frac{\int_{\Delta f} (\mu_b(f))_{dB} df}{\Delta f}$

c_w = sound speed in the reference material (*e.g.* degassed water), Δt = time difference between transit times through water with and without the object. s_b, s_1, s_2 and t_b, t_1, t_2 = thicknesses and transit times for the bone and soft tissue (Fig 3.1), respectively. s = heel thickness, A_b and A_w = ultrasound signal amplitudes in water with and without the object, respectively. T and R = transmission and reflection coefficient, respectively. Subscripts b, tb and bt refers to bone, water-bone interface and bone-water interface, respectively. μ_b = frequency dependent backscattering coefficient in bone, f = frequency and Δf = effective frequency range in use.

An alternative ultrasound method is based on the *pulse-echo* technique (Figure 3.1). In the pulse-echo measurement, a single transducer is transmitting and receiving the ultrasound signal. This enables, at least theoretically, QUS measurements from various anatomical locations which are difficult to measure with traditional through-transmission techniques. The pulse-echo technique enables determination of backscattering and reflection parameters not extractable from through-transmission measurements. These parameters (Table 3.3) have been suggested to provide quantitative information on the amount, composition and microstructure of trabecular bone [134, 63, 170, 23]. Several techniques have been introduced for the determination of backscattering parameters. These techniques utilize either a phantom [179] or a standard plane reflector [134] as the reference for the determination of backscattering. In the technique introduced by Roux *et al* [134], reflection from a standard plane reflector and sample is measured (Figure 3.2). In the determination of broadband ultrasound backscatter (BUB), the region of interest (ROI) is set at the part of the signal backscattered from inner structures of the sample. Power spectrums of the signals are calculated by using the fast Fourier transform. The integrated reflection coefficient (IRC, Table 3.3) is determined analogously although ROI is set to the part of the signal reflected from the sample surface. Both backscatter coefficient (μ_b) and reflection coefficient (R_b) are calculated by performing a log spectral subtraction of the backscattered or reflected spectra from the reference spectrum, respectively (Figure 3.3). Finally, BUB and IRC are estimated by integrating the backscatter and reflection coefficient over the effective frequency range (Table 3.3).

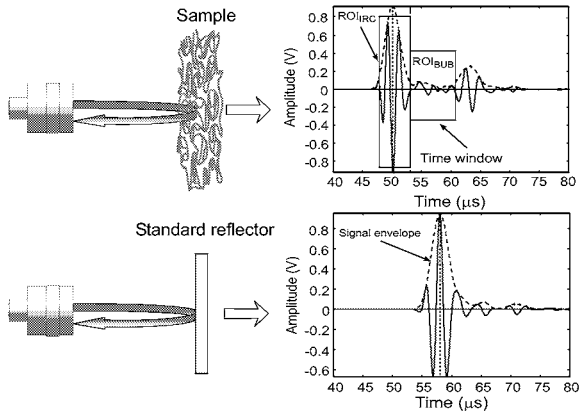

Figure 3.2: The reference method. First, a reference signal is measured from a standard reflecting target (*e.g.* polished steel plate). Secondly, reflected ultrasound signal is recorded from the sample. Region of interest (ROI) is set at the part of the signal reflected from the surface (IRC) and inner structures (BUB) of the trabecular bone sample.

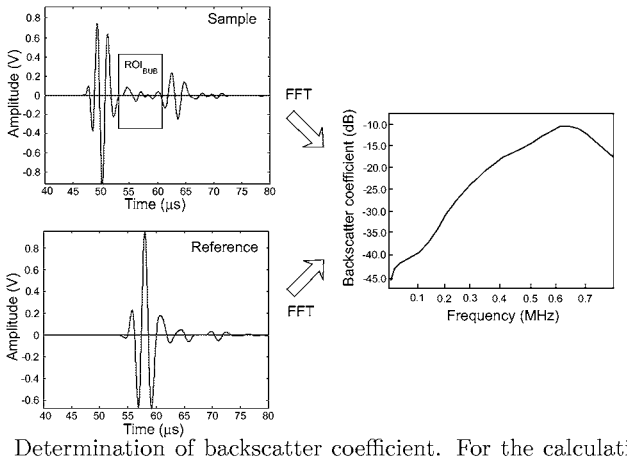

Figure 3.3: Determination of backscatter coefficient. For the calculation of power spectra, both ultrasound signals, reference and sample measurement, are Fourier transformed (FFT, fast Fourier transform). Backscatter coefficient μ_b, as a function of frequency, is determined by performing a log spectral subtraction of the backscattered spectrum from the reference spectrum.

Earlier studies have suggested that the backscattering techniques are feasible for use in the diagnostics of bone fragility [171]. Furthermore, previous studies have shown that ultrasound backscattering is associated with trabecular bone density [106, 171], microstructure [23] and composition [63], evidence of the potential of backscattering technique for bone quality characterization.

3.3 Acoustic properties of trabecular bone

In biological tissues, the loss mechanisms of ultrasound are not totally understood. It has been suggested that a significant part of the longitudinal wave absorption in soft tissues can be explained with the relaxation mechanics at the macromolecular scale of proteins [174]. The loss mechanisms can be quite different in fluid-like soft tissue and porous trabecular bone. In trabecular bone, the viscous friction between the solid mineralized matrix and the bone marrow can contribute significantly to the absorption. In addition, other mechanisms such as mode conversion from longitudinal to shear wave at the surface of the scattering particle may contribute to the attenuation [115]. The range of published values for the acoustic properties of trabecular bone is wide (Table 3.4). This variation in values reflects not only the heterogeneity of the tissue but also variation in measurement orientation and experimental methods. As discussed in chapter 3.2, different transit time detection methods affect the measured sound speed values.

Different theoretical approaches have been introduced to model ultrasound propagation through trabecular bone. The Biot theory [5] was used to explain frequency dependent attenuation in trabecular bone. Nicholson *et al* [110] theoretically assessed the experimentally discovered nonlinear relationship between BUA and BMD or porosity by using a scattering model. In addition, several theoretical models describing the frequency dependent backscattering in trabecular bone have been formulated [166, 74, 24]. In these approaches, trabecular bone has been modeled as thin cylinders [166], randomly positioned impedance fluctuations [74] or as an ensemble of small discrete scattering particles [24]. Nevertheless, our understanding of scattering phenomenon in trabecular bone is still limited.

Table 3.4: Values of ultrasound parameters for trabecular bone *in vitro*

Study	Velocity (m/s)	nBUA (dB/MHz/cm)	BUB (dB)	Orientation	Site
Bovine femur					
Njeh *et al* [117]	2171 ± 148	-	-	Mediolateral	Distal and
Bovine tibia					
Hoffmeister *et al* [64]	2284 ± 83	56.4 ± 2.8	-34.9 ± 0.7	Mediolateral	Proximal tibia
Human skull					
Fry and Barger [41]	2240 ± 180	-	-	Radial	-
Human vertebra					
Nicholson *et al* [112]	1709 ± 114	10.5 ± 6.9	-	Mediolateral	Lumbar spine
Human femur					
Njeh *et al* [118]	2409 ± 291	-	-	Mediolateral	Femoral head
Human tibia					
Han *et al* [139]	1728 ± 166	12.7 ± 6.7	-	Mediolateral	Proximal tibia
Human calcaneus					
Langton *et al* [87]	-	18.3 ± 7.4	-	Mediolateral	-
Grimm and Williams [51]	1713 ± 130	16.0 ± 9.0	-	Mediolateral	-
Laugier *et al* [89]	1517 ± 21	12.0 ± 4.3	-	Mediolateral	-
Nicholson *et al* [106]	1520 ± 36	18.4 ± 6.4	-28.8 ± 4.7	Mediolateral	-
Chaffaî *et al* [23]	1516 ± 27	12.4 ± 8.9	-22.9 ± 6.0	Mediolateral	-

nBUA = normalized BUA

CHAPTER IV

Dual energy X-ray absorptiometry

4.1 DXA technique

In dual energy X-ray absorptiometry (DXA) devices, an X-ray tube emits photons which are typically collimated into a narrow pencil beam or a fan beam. The beam passes through the patient and is registered by an X-ray detector system. The X-ray source, collimator and the X-ray detector are aligned carefully and mechanically connected to the scanning arm. As the arm moves across the patient's body, two dimensional attenuation profiles are acquired. When a DXA scan is acquired, the resulting image is effectively a pixel-by-pixel map of bone mineral density (BMD, g/cm^2). In practice, due to the variable soft tissue composition and beam hardening effects (see chapter 4.2), it is necessary to use the soft tissue regions adjacent to the bone as a baseline for the correction of the BMD values (see chapter 4.2).

4.2 Basic physics of DXA

In the DXA technique, dual energy X-ray attenuation along a path passing through the bone can be written as follows,

$$N_1 = N_{0,1}\mathrm{e}^{-M_b\alpha_{b,1}-M_s\alpha_{s,1}} \tag{4.1}$$

$$N_2 = N_{0,2}\mathrm{e}^{-M_b\alpha_{b,2}-M_s\alpha_{s,2}} \tag{4.2}$$

where N_i and $N_{0,i}$ refers to attenuated and unattenuated photon counts at X-ray energy of i. M is the mass of the constituent, $\alpha_{b,i}$ and $\alpha_{s,i}$ are the attenuation coefficients at an X-ray energy of i. Subscripts b and s denote bone and soft tissue, respectively. In DXA, soft tissue composition can be determined by measuring X-ray attenuation with both energies in soft tissue adjacent to the bone segment. X-ray attenuation can be expressed as follows:

$$N_1' = N_{0,1}'\mathrm{e}^{-M_l\alpha_{l,1}-M_f\alpha_{f,1}} \tag{4.3}$$

$$N_2' = N_{0,2}' \mathrm{e}^{-M_f \alpha_{f,2} - M_f \alpha_{f,2}} \tag{4.4}$$

where N_i' and $N_{0,i}'$ denote attenuated and unattenuated photon counts with X-ray energy i, respectively. Subscripts f and l refers to fat and lean tissue, respectively. Finally, by using equations (4.1), (4.2), (4.3) and (4.4), the bone mineral density (BMD, g/cm^2) can be determined

$$\mathrm{BMD} = \frac{\left(\frac{\alpha_{s,1}}{\alpha_{s,2}}\right) \ln\left(\frac{N_2}{N_{0,2}}\right) - \ln\left(\frac{N}{N_{0,1}}\right)}{\alpha_{b,1} - \alpha_{b,2}\left(\frac{\alpha_{s,1}}{\alpha_{s,2}}\right)} \tag{4.5}$$

The reliability of the DXA may be severely diminished due to the measurement inaccuracy arising from non-uniform soft tissue composition [1, 10, 13, 12, 34, 94, 126, 152, 153]. The composition of adjacent soft tissue is measured with the DXA. In the calculation of BMD, the soft tissue adjacent and overlying the bone are assumed to have identical compositions. Unfortunately, the soft tissue composition may vary significantly within one individual and between individuals. The difference in attenuation coefficients between fat and lean tissue is significant, being 17% and 22% for the X-ray energies of 42 keV and 68 keV, respectively [79, 128, 132]. Thus, if the assumption on identical compositions in soft tissues adjacent and overlying bone is incorrect, then the determined bone mineral density will be over- or underestimated. The inaccuracies of BMD measurements related to the non-uniform soft tissue composition have been demonstrated both experimentally and numerically [11, 38, 52, 143]. Furthermore, the bone marrow composition may vary and affect the measured BMD values [11, 143]. In current commercial scanners, the patient specific attenuation coefficient for soft tissue is calculated, although the details of the soft tissue elimination procedures are usually proprietary information [143]. Even small changes (<10%) in body weight may induce significant variation (∼2.5%) in the measured bone mineral content (BMC) [126, 152]. It has been suggested that patients with low bone density, *e.g.* elderly people, are subject to a larger relative uncertainty as compared to those with a higher bone density [52]. In specific situations, under- or overestimation of BMD, related to small non-uniform changes in soft tissue and bone marrow composition, may exceed 20% [12]. Another potential source of error in DXA measurement is related to beam hardening. In this case, lower energy photons are attenuated more effectively as compared to higher energy photons. Increasing bone thickness leads to a progressive spectrum shift to higher photon energies. Thus, the mass attenuation coefficient for bone and soft tissue will change with body thickness and therefore can vary between patients and sites within the body [7].

4.3 Diagnostic sensitivity of DXA and QUS measurements

Osteoporosis is generally diagnosed with the DXA technique (Table 4.1). The sensitivity of the method can be estimated by calculating *odds ratio* (OR) or *risk ratio* (RR) [7]. If RR or OR = 1, the measurement has no predictive value and no useful information is provided concerning fracture risk. As the RR or OR ratio becomes larger, the sensitivity of the measurement for risk of fracture is higher. When including all fractures (no site specific classification), odd ratios related to BMD measurement range between 1.4-1.5 for spine BMD [103, 6, 45], 1.4-1.6 for femoral neck BMD [103, 6, 45, 147] and 1.3-1.5 for radius BMD (both distal and proximal) [6, 32, 151, 102, 145]. For comparison, odd ratios for QUS measurements range between 1.4-1.9 for calcaneal BUA [147, 45, 151] and 1.2-1.7 for patellar SOS [145]. Further, odd ratio values of 1.6 for calcaneal SOS [151] and 1.4 phalangeal SOS [102] have been reported.

Table 4.1: Comparison of clinical DXA, peripheral DXA (pDXA), peripheral QCT (pQCT) and QUS instruments.

Device	Measurement site	Scan time	Precision	Source	Effective dose
DXA					
Lunar Expert-XL	PA spine	6, 12 s	1.7-1.9% (L1-L4) [86]	40 kV and 70 kV	20 μSv
	Femur	6,12 s	1.6-2.6% (femoral neck) [86]	(K-edge filter)	
	Whole body	240 s			
	Forearm	10 s			
	Morphometry	40 s			
Hologic QDR-4500A	PA spine	10, 30, 60 s	1.1% (lumbar spine) [57]	100 and 140 kVp	3 μSv
	Femur	10, 30 ,60 s	1.3% (total hip) [57]	(switched kV)	
	Whole body	180 s	1.0% (distal forearm) [57]		
	Lateral spine	120 s			
	Forearm	30 s			
	Morphometry	10 s, 600 s			
Norland Eclipse	PA spine	120 s	<1.0% (spine)	47 kV and 80kV	20 μSv
	Femur	180 s	<1.2% (hip)	(K-edge filter)	
	Whole body	300 s	(reported by manufacturer)		
	Forearm	180 s			
Lunar Prodigy	AP spine	30 s	<1.0% (spine)	38 kV and 62 kV	1.35 μSv
	Femur	30 s	<1.0% (femur)	(K-edge filter)	1.13 μSv
	Whole body	270 s	<1.0% (whole body)		
	Forearm	-	(reported by manufacturer)		
	Lateral spine				
	Vertebra				
pDXA					
Lunar PIXI	Calcaneus	5 s	1.0-1.5%	55 kVp and 80 kVp	<2 μSv
	Distal forearm		(reported by manufacturer)	(switched kV)	
Norland Apollo	Calcaneus	15 s	typical 1.8%	28 kV and 48 kV	<2 μSv
			(reported by manufacturer)	(K-edge filter)	
pQCT					
Stratec XCT-2000L	Tibia	90 s (radius)	0.82% (Trabecular density) [105]	56-60 kV	30 μSv
	Forearm		1.1% (Cortical density) [105]		
Stratec XCT-3000	Tibia	90 s	1.4-1.6% (Trabecular density) [16]	59-61 kV	<2 μSv
	Forearm		1.3% (Cortical density) [16]		
QUS					
Hologic Sahara	Calcaneus	<10 s	BUA = 3.7% [115]	0.6 MHz unfocused	none
			SOS = 0.22% [115]		
			Est. heel BMD = 3.0% [115]		
			QUI = 2.6% [115]		
CUBA clinical	Calcaneus	120 s	VOS = 0.50% [115]	1 MHz unfocused	none
			BUA = 2.0% [115]		
UBIS 5000	Calcaneus	60-120 s	SOS = 0.25% [115]	0.5 MHz focused	none
			BUA = 0.50% [115]		
Lunar Achilles+	Calcaneus	180-240 s	SOS = 0.30% [115]	0.5 MHz unfocused	none
			BUA = 1.7% [115]		
			Stiffness = 1.7% [115]		

CHAPTER V

High resolution computed tomography

5.1 QCT technique

Typical analysis of computed tomography (CT) images is qualitative, however, the data it provides on volumetric densities (g/cm^3) yields valuable information and is known as quantitative computed tomography (QCT). QCT enables determination of mineral density, cortical thickness, bone size and shape. The peripheral QCT (pQCT) technique enables determination of these parameters at peripheral skeletal sites, *e.g.* radius and tibia. As compared to conventional QCT, pQCT scanners provide inexpensive means for quantitative evaluation of peripheral bones. A high resolution computed tomography, *i.e.* microCT, technique has been introduced for *in vitro* use [119, 37, 36]. As compared to QCT and pQCT, microCT-technique provides more detailed high resolution information about bone structure, *e.g.* trabecular thickness, spacing and other parameters describing the trabecular architecture. In addition, the microCT- technique enables finite element (FE) modeling of the mechanical properties of the bone specimen based on the fine trabecular architecture [161, 82].

5.2 Morphological analyses

MicroCT and high resolution QCT techniques enable morphological analyses of trabecular structure. The first step in morphological analyses is the segmentation process. In the analysis of trabecular bone morphology, the segmentation of the original grayscale data sets is used to separate bone from other tissues. The most widely used segmentation techniques utilize global thresholds in which a single CT number is chosen with histogram techniques [30]. All voxels (3D pixels) having a CT value above the threshold are defined as bone and the remaining voxels as non-bone. The choice of the segmentation method has a considerable influence on the calculated morphological parameters [72, 135, 55, 22, 30]. Recent studies have

demonstrated that the segmentation can be improved by using the local threshold values instead of the global threshold values [162].

Subsequently, the morphological parameters can be determined from the segmented three-dimensional data sets. There are a number of techniques available for the calculation of structural parameters [58, 84, 135, 59, 120, 119, 30, 49, 121, 56]. Here, only a brief description of some typical techniques is presented. The "marching cube" algorithm [96] has been introduced for modeling bone surface using continuous triangles (surface triangulations). Bone surface (BS) is defined as a total area of the triangles. Bone volume (BV) is estimated by summing the volume of the voxels in trabeculaes. Total tissue volume (TV) is estimated by summing the volumes of all voxels in the calculation volume. From this information, bone volume fraction (BV/TV) and bone surface-to-volume ratio (BS/BV) can be calculated. The structural model index (SMI) is a measure of the predominant shape of trabeculae in bone tissue: SMI values of 0 and 3 refer to ideal plate-like and rod-like structures, respectively. SMI can be calculated by determining the area-averaged mean curvature (H) [75]:

$$\langle H \rangle = \frac{1}{2} \frac{\int\int(\kappa_1 + \kappa_2)da}{\int\int da} \tag{5.1}$$

where da is the area element of the bone surface and κ_i (1 and 2) is the principal curvature of the bone surface (Figure 5.1).

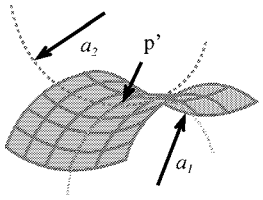

Figure 5.1: A schematic presentation of a saddle-shaped surface showing the two tangential circles (a_1 and a_2 are the radii of the circles) used to define the principal curvatures ($\kappa_1 = 1/a_1$ and $\kappa_2 = 1/a_2$) at any point $\underline{p}$ on the surface.

Using equation (5.1) SMI can be written as follows [75]

$$\text{SMI} = \frac{12 \cdot \langle H \rangle \cdot \text{BV}}{\text{BS}} \tag{5.2}$$

Connectivity is a measure of connectivity in the three-dimensional architecture. *Euler-Poincaré* characteristic (Euler number), χ, is used in the determination of

connectivity. The gaussian curvature (K), which is a measure of the curvedness of a surface, can be defined as [75]:

$$\langle K \rangle = \frac{\int\int(\kappa_1 \cdot \kappa_2)da}{\int\int da} \tag{5.3}$$

and the relationship between Euler number χ and gaussian curvature (K) can be written as [75]:

$$\chi = \frac{\langle K \rangle \cdot \mathrm{BS}}{2\pi} \tag{5.4}$$

where χ describes the complexity of network connectivity: the more negative χ becomes, the more complex is the structure. On the other hand, Euler number χ is related to the connectivity and the number of bone particles and marrow cavities [119]:

$$\chi = \beta_0 - \beta_1 + \beta_2 \tag{5.5}$$

where β_0 is the number of bone particles, β_1 is the connectivity and β_2 is the number of cavities encapsulated within the bone. Generally, trabecular bone is assumed to be one fully-connected structure without any isolated components (β_0=1) and no marrow cavities are considered to exist encapsulated within bone nor being apart of from the main marrow space (β_2=0). The connectivity (β_1) can be solved from the equation (5.5) [119]:

$$\text{Connectivity} = 1 - \chi \tag{5.6}$$

Mean trabecular bone thickness (Tb.Th.) and separation (Tb.Sp.) can be determined directly from 3D data [58] without model assumptions on the trabecular structure, *e.g.* assumption of plate-like structure [124]. Hildebrand and Rüegsegger [58] suggested that the mean trabecular thickness ($\bar{\tau}$) can be defined without model assumption by determining the arithmetic mean value of the local thicknesses of the individual trabeculae [58]:

$$\bar{\tau} = \frac{1}{\mathrm{Vol}(\Omega)} \int\int\int_{\Omega} \tau(\underline{x}) \mathrm{d}^3\underline{x} \tag{5.7}$$

where

$$\mathrm{Vol}(\Omega) = \int\int\int_{\Omega} \mathrm{d}^3\underline{x}$$

and $\Omega \subset \mathbf{R}^3$ is the set of all points in the trabecular network under investigation. The local thickness is defined as a diameter of the largest sphere which contains the point ($\underline{p}$) and which fits completely inside the trabeculae (Figure 5.2).

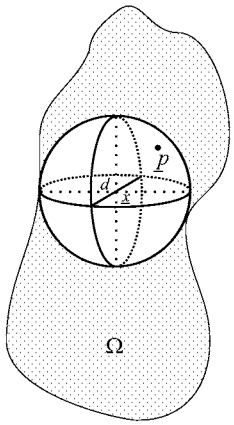

Figure 5.2: Local thickness $\tau(\underline{p})$ of a structure Ω determined by fitting maximal spheres to the trabeculae. The sphere must enclose the point $\underline{p}$ and fit entirely within the trabecular surfaces. d = diameter of the sphere and $\underline{x}$ = center of the sphere.

The degree of anisotropy (DA) can be determined by using the mean intercept length (MIL) analysis. The mean intercept length is determined by placing a line through the 3D segmented image volume and dividing the length of the line through the 3D structure by the number of times the line intercepts the trabeculae. For MIL analysis, a 2D grid of lines is placed through a 3D structure in a large number of 3D angles. The MIL for each direction is calculated as a mean MIL of all lines in the grid. 3D distribution of MIL lengths are visualised as an ellipsoid (Figure 5.3). Next, the fitted ellipsoid is described with a tensor or second order tensor. The tensor describing the anisotropy ellipsoid is an orthogonal tensor. Next, a 3x3 matrix of eigenvectors, describing the 3D angles of the three axis of the ellipsoid, is determined. In addition, three eigenvalues, representing the relative lengths of bone intercepts in each three axes described by the eigenvectors, are calculated. Finally, DA is calculated as the maximum eigenvalue divided by the minimum eigenvalue:

$$\mathrm{DA} = \frac{\mathrm{eigenvalue}_{\mathrm{max}}}{\mathrm{eigenvalue}_{\mathrm{min}}} \tag{5.8}$$

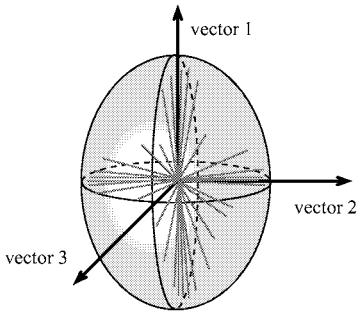

Figure 5.3: An ellipsoid fitted to the 3D distribution of MIL lengths measured over large number of 3D angles. The fitted ellipsoid has 3 vectors which are orthogonal. A tensor of 9 eigenvectors (3x3 matrix) describes the directions of each vector.

Chapter VI

Potential significance of QUS technique

As a limitation, DXA involves ionizing radiation and measures only areal BMD (g/cm^2). Axial DXA devices are rather expensive, immobile instruments. Obviously, quantitative techniques also capable of measuring other bone characteristics, in addition to the amount of bone, and which would be both mobile and inexpensive would have major clinical applications. QUS devices are less expensive and involve no ionizing radiation. Moreover, clinical QUS devices have been demonstrated to identify patients with increased risk of fractures as well as the axial BMD measurement [39]. Thus, the QUS technique may be feasible for screening large populations with an increased risk of osteoporosis.

The interrelationships between QUS parameters and BMD have been studied extensively (see review by Njeh *et.al.* [113]). The linear correlations between BMD and BUA or SOS have ranged from $r = 0.34$ to $r = 0.87$ [113]. In addition, the linear association between BMD and ultrasound backscattering parameters have ranged from $r = 0.34$ to $r = 0.50$ *in vivo* [170, 134] and from $r = 0.67$ to $r = 0.89$ *in vitro* [24, 106, 172]. It has been recognised that BMD alone can predict 80% of the bone fracture susceptibility [69, 97, 131]. The remaining 20% may be accounted for by the bone structure and composition. In trabecular bone, QUS parameters exhibit anisotropy [54, 109, 117] as well as exhibit a significant association with trabecular microstructure [46, 24, 28]. This suggests that QUS can also reflect bone structural characteristics. It has been proposed that QUS can add predictive value beyond that of density and may be useful in the estimation of the mechanical properties of trabecular bone [114].

CHAPTER VII

Aims of the present study

The DXA method only measures bone mineral density, neglecting the trabecular structure and organic composition. In addition, variable bone size as well as the unknown amount and composition of soft tissue and bone marrow may diminish the quality of both clinical DXA and QUS measurements. Novel ultrasound backscattering approaches have been claimed to provide additional information not available from current clinical DXA or QUS devices. However, the relationships between backscattering and mechanical or structural properties of bone are unclear. Furthermore, the most sensitive backscattering parameters and the optimal ultrasound frequency have not been thoroughly investigated.

To clarify these issues the present study aimed to

- compare DXA, dual energy X-ray laser (DXL) and ultrasound transmission techniques for the assessment of bone mineral density,
- determine the optimal ultrasound parameters for the assessment of volumetric density, structure and mechanical properties of trabecular bone,
- reveal the most sensitive frequency range for ultrasonic prediction of the mechanical and structural properties of trabecular bone,
- compare capabilities of ultrasound through-transmission and pulse-echo techniques to predict of volumetric bone density, structure and mechanical properties.

CHAPTER VIII

Materials and Methods

This thesis consist of four independent Studies I - IV.

8.1 Materials

For Study I, 38 subjects (aged 59.7 ± 9.4 years, 18 males and 20 females) were recruited. In addition, to determine the short-time precision of the instrument, 24, 11 and 10 subjects were measured three times with three devices - DXL Calscan, Hologic Sahara and Lunar PIXI, respectively.

For Study II, fresh intact bovine knee joints were obtained from the local slaughter house (Atria Lihakunta Oyj, Kuopio, Finland) a few hours after slaughtering. Cylindrical trabecular bone samples (n = 41, d = 25.4 mm, h = 14.2 mm) were prepared from four anatomical locations: femoral medial (n = 10) and lateral (n = 10) condyles, femoral trochanter major (n = 10) and femoral caput (n = 11). The plugs were drilled and detached in the medio-lateral direction using a hollow drill bit. Next, the faces of the cylindrical samples were cut perpendicular with an ISOMET© low speed diamond saw (Buehler, IL, USA). Samples were immersed in phosphate buffered saline (PBS), stored in a freezer (-20 °C) and thawed just before measurements.

In Studies III and IV, human cadaver knees (n = 10 and 13, age = 60 ± 18 and 58 ± 20 years, 10-12 males and one female, respectively) were collected with the permission of the National Authority of Medicolegal Affairs (Helsinki, Finland, permission 1781/32/200/01). Cylindrical plugs of trabecular bone (n = 26, d = 16 mm, h = 8 mm) were prepared from femoral medial condyle (n = 10), femoral groove (n = 6) and tibial medial plateau (n = 10). The plugs were drilled and the faces were cut perpendicular with a micro-grinding system (Macro Exakt 310 CP, Exakt, Hamburg, Germany). Finally, the samples were immersed in PBS, stored in a freezer (-20 °C) and thawed just before the measurements.

The materials used in the Studies are summarized in Table 8.1.

Table 8.1: Summary of materials used in Studies I - IV.

Study	Materials	n	Geometry	Size	Site
I	Randomly selected patients	38 18 males, 20 females	- - -	- - -	Calcaneus Lumbar spine Total body Femoral neck
II	Bovine trabecular bone	41	Cylindrical samples	d = 25.4 mm h = 14.2 mm	FMC FLC FC FTM
III	Human trabecular bone	20	Cylindrical samples	d = 16 mm h = 8 mm	FMC TMP
IV	Human trabecular bone	26	Cylindrical samples	d = 16 mm h = 8 mm	FMC TMP FG

Explanation of the abbreviations:

FMC	Femoral medial condyle
FLC	Femoral lateral condyle
FC	Femoral caput
FTM	Femoral trochanter major
TMP	Tibial medial plateau
FG	Femoral groove

8.2 Methods

The methodology used in Studies I-IV is summarized in Table 8.2.

8.2.1 Quantitative ultrasound methods

In Study I, a commercial ultrasound instrument was utilized (Hologic Sahara, Hologic Inc., MA, USA). The Hologic Sahara comprises two 0.6 MHz unfocused ultrasound transducers and utilizes the through-transmission geometry in the measurement of calcaneal acoustic properties (Figure 3.1). In Studies II, III and IV, trabecular bone samples were measured with the UltraPAC system (Physical Acoustic Co., NJ, USA) in through-transmission and pulse-echo geometry. The UltraPAC system consists of a 500 MHz A/D-board and a 0.2-100 MHz pulser-receiver board. The system is controlled with custom-made software based on LabVIEW (version 6i, National Instruments, TX, USA). For Studies III and IV, the system was equipped with a tank and scanning drives (Figure 8.1). In Studies III and IV, five pairs of focused broadband ultrasound transducers (center frequencies of 0.5 MHz, 1 MHz, 2.25 MHz, 3.5 MHz and 5 MHz) covering a wide frequency range (0.2-6.7 MHz) were used. For Studies II, III and IV sample holders enabling specific measurement geometry were designed and constructed (Figure 8.1). In Study II, the point-wise BUB and IRC measurements were taken from both sides of the sample. The final values were calculated as an average of these measurements. In Studies III and

Table 8.2: Summary of the methods and determined parameters in Studies I - IV.

Study	Method	Device	Parameters	Energy/Frequency
I	DXA	Lunar DPX-IQ	$BMD_{lumbar\ spine}$ $BMD_{femoral\ neck}$ $BMD_{total\ body}$	38 kV and 70 kV
	pDXA	Lunar PIXI	$BMD_{calcaneus}$	55 kVp and 80 kVp
	DXL	DXL Calscan	$BMD_{calcaneus}$ Heel thickness	30 kV and 70 kV
	QUS	Hologic Sahara	$BUA_{calcaneus}$ $SOS_{calcaneus}$ 'Estimated BMD'	0.6 MHz
II	DXA	Lunar Expert-XL	BMD	40 kV and 70 kV
	QUS	UltraPAC	nBUA, SOS, BUB, IRC	0.5 MHz
	Mechanical testing	Matertest	E, σ_{max}, σ_y, ϵ_y, resilience	-
III	DXA	Lunar Prodigy	BMD	76 kV (K-edge filter)
	QUS	UltraPAC	nBUA, SOS, AA, BUB, IRC	0.5 MHz, 1 MHz, 2.25 MHz, 3.5 MHz, 5 MHz
	Mechanical testing	Zwick 1484	E, σ_{max}, resilience	-
IV	microCT	SkyScan 1072	BV/TV, Tb.Th, Tb.Sp., BS/BV, SMI, DA, connectivity	80 kV or 100 kV
	QUS	UltraPAC	nBUA, SOS, AA, BUB, IRC	0.5 MHz, 1 MHz, 2.25 MHz, 3.5 MHz, 5 MHz

Abbreviations and symbols for parameters:

BMD	Bone Mineral Density
BUA	Broadband Ultrasound Attenuation
nBUA	normalized BUA
AA	Average attenuation
SOS	Speed of Sound
BUB	Broadband Ultrasound Backscatter
IRC	Integrated Reflection Coefficient
E	Young's modulus
σ_{max}	Ultimate strength
σ_y	Yield stress
ϵ_y	Yield strain
BV/TV	Bone volume fraction
Tb.Th, Tb.Sp.	Trabecular thickness and spacing, respectively
BS/BV, SMI	Bone surface-to-volume ratio and Structural Model Index, respectively
DA	Degree of Anisotropy

IV, ultrasound signals in both through-transmission and pulse-echo geometry were recorded across a scan area of 16 mm $\times$ 16 mm (Figure 8.1). Pixel size was 0.25 mm^2 for all transducers except at 5 MHz, for which the pixel size was set to be 0.09 mm^2. A region of interest (ROI, circle area = 35 mm^2) was set to the center of each sample. The final values were determined as an average of the values inside the ROI.

Through-transmission method

Normalized BUA (nBUA), average attenuation and SOS were measured using the through-transmission technique and applying the substitution method [88]. In the

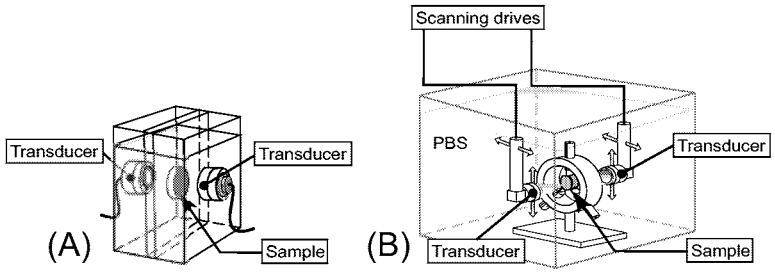

Figure 8.1: Schematic presentation for ultrasound measurement geometries. The samples were placed always in the focal plane of the transducers. (A) In Study II, bovine trabecular bone samples were measured with two focused broadband ultrasound transducers (center frequency of 0.5 MHz) that were facing each other. During the measurements, the samples were immersed in temperature controlled (37 ± 1 °C) water bath. (B) In Studies III and IV, the human trabecular bone samples were measured with five pairs of ultrasound transducers (center frequencies of 0.5 MHz, 1 MHz, 2.25 MHz, 3.5 MHz and 5 MHz) across a scan area of 16 mm × 16 mm in a vacuum degassed PBS bath. During the measurements, the PBS bath was maintained at room temperature (between 20.1 and 23 °C).

substitution technique, the pulse transit time and pulse amplitude spectrum are recorded in the presence and absence of the sample. Subsequently, an attenuation spectrum is determined as the logarithm of the difference of these spectra. Average attenuation was calculated as presented in Table 3.3. BUA was determined as a slope of the linear fit to the linear part of the attenuation spectrum: Study II: 0.3-0.6 MHz, Studies III and IV: 0.3-0.6 MHz, 0.7-1.5 MHz, 1-2.8 MHz, 1-3 MHz and 1.5-3 MHz for center frequency of 0.5 MHz, 1 MHz, 2.25 MHz, 3.5 MHz and 5 MHz, respectively. Finally, nBUA was calculated by normalizing BUA with the sample thickness. For Study II and Studies III/IV, the sample thickness used in the calculations was measured using the pulse-echo technique and a micrometer (Mitutoyo Co., Kawasaki, Japan), respectively. SOS was calculated with the time of flight (TOF) method [113]. In the time-of-flight technique, the pulse transit time through the water bath is recorded with and without the sample using a constant distance between the transducers. In Study II, the pulse transit time was computed as the mean of the zero crossing times before and after the maximum of the signal envelope [130]. In Studies III and IV, the pulse transit time was determined with the threshold method [107] using a 20% threshold value.

Pulse-echo method

BUB and IRC were measured using a single transducer in the pulse-echo mode. Both parameters were determined with the reference method [134, 27] in which two signals are acquired. First, the reference signal was recorded by measuring reflected

ultrasound signal from a standard reflecting target (water-air interface and stainless steel plate (d = 32 mm, h = 10 mm) in Study II and Studies III/IV, respectively). Standard reflectors were placed at a distance corresponding to the center of the sample. Next, ultrasound reflection from the sample placed in the focal plane of the transducers was measured (Figure 3.2). BUB and IRC were determined by integrating the backscatter or reflection coefficient in the effective frequency range of the transducer (Table 3.3). In Study II, the effective frequency range was 0.2-0.6 MHz. In Studies III and IV, the effective frequency ranges (-6 dB) were 0.28-0.69 MHz, 0.70-1.46 MHz, 1.53-3.80 MHz, 2.03-5.50 MHz and 3.23-6.66 MHz for 0.5 MHz, 1 MHz, 2.25 MHz, 3.5 MHz and 5 MHz center frequencies, respectively. In Study III and IV, the backscatter coefficients were adjusted with the correction factors [106] to compensate for the attenuation in the human trabecular bone.

8.2.2 X-ray methods

Dual energy X-ray laser method

In Study I, calcaneal BMD values were measured with the DXL Calscan (Demetech AB, Solna, Sweden) instrument. In the dual energy X-ray laser (DXL) method, a heel is scanned with two X-ray energies (35 keV and 70 keV). In addition, a laser reflection technique is used to determine the heel thickness. By measuring the heel thickness (s_h), the bone thickness (thickness of solid hydroxyapatite, s_b) can be determined without assumptions about the soft tissue composition [77]:

$$s_b = \frac{(K_1\rho_f\alpha_{f,2} - K_2\rho_f\alpha_{f,2})\Delta_{l,f} - (K_2 - \rho_f\alpha_{f,2}h_t)D_{l,f}}{D_{b,f}\Delta_{l,f} - D_{l,f}\Delta_{b,f}} \tag{8.1}$$

where

$$\begin{aligned}
D_{b,f} &= \rho_b\alpha_{b,1}\rho_f\alpha_{f,2} - \rho_b\alpha_{b,2}\rho_f\alpha_{f,1} \\
D_{l,f} &= \rho_l\alpha_{l,1}\rho_f\alpha_{f,2} - \rho_l\alpha_{l,2}\rho_f\alpha_{f,1} \\
\Delta_{b,f} &= \rho_b\alpha_{b,2} - \rho_f\alpha_{f,2} \\
\Delta_{l,f} &= \rho_l\alpha_{l,2} - \rho_f\alpha_{f,2} \\
K_1 &= \ln\left(\tfrac{N_{01}}{N_1}\right) \\
K_2 &= \ln\left(\tfrac{N_{02}}{N_2}\right)
\end{aligned}$$

where N_1 and N_2 are the photon counts recorded after X-rays have transmitted through the heel, N_{01} and N_{02} are unattenuated photon counts at X-ray energies of 30 keV and 70 keV, respectively. s is the thickness of tissue component. Subscripts b and t refer to bone and heel, respectively. $\alpha_{i,j}$ is the mass attenuation coefficient (cm^2/g). Subscripts $b, 1/b, 2$, $l, 1/l, 2$ and $f, 1/f, 2$ refer to bone, lean tissue and fat at X-ray energies of 30 keV and 70 keV, respectively. ρ_i (g/cm^3) is the physical density of a given (i) tissue component.

Finally, by knowing the density of bone tissue (ρ_b), areal bone mineral density (BMD, g/cm^2) can be determined

$$\text{BMD} = \rho_b s_b. \tag{8.2}$$

Dual energy X-ray absorptiometry

In Study I, BMD of calcaneus, proximal femur, lumbar spine (L2-L4) and total body were determined using the Lunar PIXI and DPX-IQ (Lunar Co./GE medical, Wessling, Germany) instruments, respectively. All measurements were conducted according to the manufacturer's instructions.

In Study II, BMDs of the bovine trabecular bone samples were measured with the Lunar Expert-XL (Lunar Co., Madison, WI, USA) instrument. During the measurements, the samples were immersed in PBS bath at a constant depth. Volumetric BMD (vBMD) values were calculated by normalizing the areal BMD values with the sample thickness, as determined with a micrometer (Mitutoyo Co., Kawasaki, Japan).

In Study III, the human trabecular bone samples were measured with the Lunar Prodigy instrument (GE Medical, Wessling, Germany). BMD values of the samples were determined using the AP spine measurement protocol. During the measurements, the samples were immersed in a water bath at a constant depth.

In Studies II and III, the DXA measurements were conducted in a direction perpendicular to the parallel ends of the cylindrical samples.

MicroCT

In Study IV, microstructural characteristics of the trabecular bone samples were determined with a high resolution computed tomography (microCT) instrument (Skyscan 1072, Skyscan, Aartselaar, Belgium). Each microCT image (voxel size 18 $\times$ 18 $\times$ 18 μm^3) was segmented using a local threshold method [162] in order to obtain accurate 3-D data sets. From the segmented 3-D data sets, seven microstructural parameters were calculated based on the true, unbiased and assumption-free 3-D methods. Trabecular bone volume fraction (BV/TV, %) and bone surface-to-volume ratio (BS/BV, mm^{-1}) were quantified. A direct 3-D analysis [58], without any model-assumption about the trabecular structure, was utilized to calculate the mean trabecular bone thickness (Tb.Th., μm^{-1}) and spacing (Tb.Sp., μm^{-1}). The structural model index (SMI) was determined according to Hildebrand and Ruegsegger [59]. Connectivity (mm^{-3}) was calculated along Odgaard and Gundersen [120]. Finally, the degree of anisotropy (DA) was defined as the ratio between the maximal and minimal eigenvalues of the fabric tensor of the architecture [119].

8.2.3 Mechanical testing

In Studies II and III, 12.5 kN and 200 kN servo-hydraulic material testing devices (Matertest (Matertest Oy, Espoo, Finland) and Zwick 1484 (Zwick GmbH & Co. KG, Ulm, Germany)) were used, respectively.

In Study II, cylindrical plugs (d = 19 mm) drilled from the center of the original samples were used in the mechanical measurements. Throughout the testing, the samples were immersed in a PBS bath. First, a small prestress (0.13 MPa) was applied for 2 min. Subsequently, a good contact between the loading platens and the samples was ensured by performing five sequential non-destructive preconditioning cycles up to 0.7% strain. Finally, the samples were destructively compressed to 4.5% strain at a strain rate of 3.5 $\times$ 10^{-3} s^{-1}.

In Study III, a teflon foil was inserted between the platens and bone surfaces to ensure frictionless contact. The samples were moistened during the mechanical testing to avoid dehydration. Before the destructive testing, samples were subjected to a small prestress (25 kPa) and preconditioned with five consecutive non-destructive cycles to 0.5% strain. Finally, the samples were compressed at a strain rate of 4.5 $\times$ 10^{-3} s^{-1} to a destructive strain of 5%.

In Studies II and III, Young's modulus was calculated as a slope of linear fit to the stress-strain curve in the range from 45% to 60% of the maximum stress [91]. Yield point is often defined as the point where the stress-strain curve begins to become nonlinear [70, 68, 71]. In Studies II and III, an offset method [156, 155, 160], using an offset of 0.2%, was used to detect the yield point. Irregularities in the sample surface and misalignment of the compressive platens may result in a nonlinear toe section at the beginning of the stress-strain curve [154, 21, 91]. Therefore, zero strain was defined as the intersection between the x-axis of the stress-strain curve and the tangent line calculated to the 15% yield stress. This point was chosen since it was observed that the nonlinear toe region of the stress-strain curve ended at approximately 15% of the yield stress. Ultimate strength was determined as the maximum stress recorded during the test. Resilience was calculated as described in section 2.2.

8.2.4 Numerical methods

In Study I, an *in vivo* calcaneal DXA measurement was simulated in order to investigate the inaccuracies related to the determination of BMD. In the simulations, constant heel thickness (d = 52.4 mm) was applied throughout the measurement area. A typical fat-to-lean tissue ratio (0.32 [104]) was used at the bone region. A wide range of BMD values (0.4-1.4 g/cm^2) and normalized fat-to-lean tissue ratios (0.1-3, equation 8.3) were used in the simulations. The normalized fat-to-lean tissue ratio was defined as follows:

$$\text{Normalized fat-to-lean tissue ratio} = \frac{\text{Fat}_{\text{baseline}}(\%)}{\text{Fat}_{\text{bone region}}(\%)} \times 100\% \tag{8.3}$$

where $\text{Fat}_{\text{baseline}}$ (%) and $\text{Fat}_{\text{bone region}}$ (%) are the fat contents of soft tissue in baseline and bone region, respectively. Attenuation coefficients of glycerol trioleate (triolein), water and calcium hydroxyapatite were used in the simulations to correspond to the attenuation coefficients of fat, lean tissue and bone, respectively [76]. Values for mass attenuation coefficients and densities were collected from the literature [76]. X-ray energies of 40 keV and 70 keV were used in the simulations. These energies are typically applied in clinical DXA devices [52]. To demonstrate the potential inaccuracies in BMD related to the non-uniform soft tissue composition, the relative error in BMD was defined as follows

$$\text{Error}(\%) = \frac{\text{BMD}_{\text{estimated}} - \text{BMD}_{\text{true}}}{\text{BMD}_{\text{true}}} \times 100\% \tag{8.4}$$

where $\text{BMD}_{\text{estimated}}$ and BMD_{true} refer to calculated and true BMD values, respectively. Simulations were performed with Matlab 5.3 (The Mathworks Inc., Natick, MA, USA) using a custom analysis function designed for the application.

In Study IV, a commercial simulation package (Wave 2000 Pro, Cyberlogic Inc., NY, USA) was used to simulate acoustic wave propagation through trabecular bone samples. In the software, the 2-D acoustic wave equation is solved using the finite difference technique [100]. The numerical solution is based on an algorithm published by Schechter *et al* [137]. The specific simulated acoustic equation is given by:

$$\rho \frac{\partial^{\theta} \mathbf{w}}{\partial^{\theta} t} = \left[\delta + \eta \frac{\partial}{\partial t}\right] \Delta^{\theta} \mathbf{w} + \left[\gamma + \delta + \Phi \frac{\partial}{\partial t} + \frac{\eta}{3} \frac{\partial}{\partial t}\right] \Delta(\Delta \cdot \mathbf{w}) \tag{8.5}$$

In the equation 8.5, which applies in an isotropic elastic region, ρ = material density (kg/m^3), γ = first Lame constant (N/m^2), δ = second Lame constant (N/m^2), Δ = Laplace operator, η = shear viscosity (Ns/m^2), Φ = bulk viscosity (Ns/m^2), t = time (s) and $\mathbf{w}$ = two dimensional vector of displacement of the medium.

Three-dimensional (3-D) images were reconstructed from segmented 2-D microCT images using VoxBlast 3.1 (VayTec Inc., IA, USA) software. For the acoustic simulations, 2-D slices extracted as an axial plane of the 3-D image were imported to the simulation software. Pixel size ($18 \times 18 \times 18$ μm^3) was set to be identical with the original microCT image. Trabecular bone was considered to consist of two materials: trabeculae (cortical bone) and inner/outer coupling medium (water 25°C). The acoustic properties for the cortical bone and water were adopted from the material library of the simulation software. Simulations were conducted with same kind of measurement geometry as used in the experimental measurements (Study III, IV). The ultrasound transducers used in the simulations were matched with the

transducers (center frequency of 2.25 MHz) used in the experimental measurements. SOS and average attenuation were calculated from the simulated output similarly as in experimental measurements (section 8.2.1).

8.2.5 Statistical analyses

In Study I, paired samples t-test was used to investigate the differences between BMD values determined with the DXL Calscan and Lunar PIXI. The short term precision of the instruments was estimated in terms of a coefficient of variation (CV%) [44] and a standardized coefficient of variation (sCV%) [116]. Pearson's correlation analysis was used to calculate linear correlation coefficients. The statistical significance of difference between the correlation coefficients was determined using the Student's t-test [142]. Bland-Altman plot was used to demonstrate the agreement of the two measurement techniques [8].

In Study II, the reproducibility of ultrasound measurements was investigated by measuring 10 samples each 3 times and calculating the CV% and sCV%. To reveal the topographical variation in the measured parameters, the nonparametric Kruskall-Wallis H test was applied. A stepwise linear regression was used to investigate the ability of ultrasound parameters and their combinations to predict the mechanical properties and density of bovine trabecular bone.

In Study III, the nonparametric Friedman test was used to determine the variation of ultrasound parameters between different center frequencies. Pearson's correlation analysis was used to reveal associations between the acoustic and mechanical parameters. A stepwise linear regression analysis was utilized to investigate the ability of ultrasound parameters and their combinations to estimate the density and mechanical properties of human trabecular bone.

In Study IV, linear correlation coefficients were calculated using Pearson's correlation analysis. Principal component analysis with Varimax rotation was applied to reduce the dimensionality of the original microstructural data. A stepwise linear regression analysis was used to investigate the relationships between the structural parameters or their combination with the ultrasound parameters.

SPSS 8.0 and 11.5 (SPSS Inc., Chicago, IL, USA) softwares were used for statistical analysis in Studies I/II and III/IV, respectively.

Chapter IX
Results

9.1 Dual energy X-ray laser assessment of bone mineral density

In vivo reproducibilities (sCV%) of the DXL Calscan and Lunar PIXI BMDs were similar (1.5% and 1.6%, respectively; Table 9.1).

Table 9.1: Reproducibilities of the QUS and pDXA parameters as determined in Studies I-IV.

Parameter	CV (%)	sCV (%)
in vitro		
nBUA	3.5	2.1
SOS	0.3	0.5
IRC	1.6	1.5
BUB	2.1	3.5
in vivo		
BUA_{Sahara}	4.1	3.6
SOS_{Sahara}	0.3	2.8
$BMD_{Calscan}$	1.2	1.5
BMD_{PIXI}	1.3	1.6

Although the linear correlation ($r^2 = 0.78$, $n = 36$, $p < 0.01$) between DXL Calscan and Lunar PIXI was significant, the BMD values measured with DXL Calscan were 19% lower than those obtained with Lunar PIXI (0.452 ± 0.095 g/cm^2 vs. 0.565 ± 0.114 g/cm^2, respectively). The difference increased as a function of heel thickness ($r^2 = 0.37$, $n = 36$, $p < 0.01$) and body mass index ($r^2 = 0.17$, $n = 36$, $p < 0.02$, Figure 9.1). The strength of associations between the quantitative ultrasound parameters and BMD values measured with DXL Calscan was moderate ($r^2 = 0.52$, $n = 34$, $p < 0.01$ for BUA, $r^2 = 0.53$, $n = 34$, $p < 0.01$ for SOS and $r^2 = 0.52$, $n = 34$, $p < 0.01$ for 'estimated BMD').

The linear correlations between axial BMD values and calcaneal BMD values measured with DXL Calscan or Lunar PIXI were significant ($r^2 = 0.61$-0.76, $n = 38$ and $r^2 = 0.52$-0.74, $n = 36$, $p < 0.01$, respectively). The corresponding linear

correlations between axial BMD and acoustic parameters, as determined with Hologic Sahara, were not statistically different (r^2 = 0.29-0.45, n = 34-36, $p < 0.01$) as compared to calcaneal BMD.

Numerical simulations revealed a clear increase in the relative BMD error as the normalized fat-to-lean tissue ratio increased or/and the true BMD value decreased (Figure 9.1).

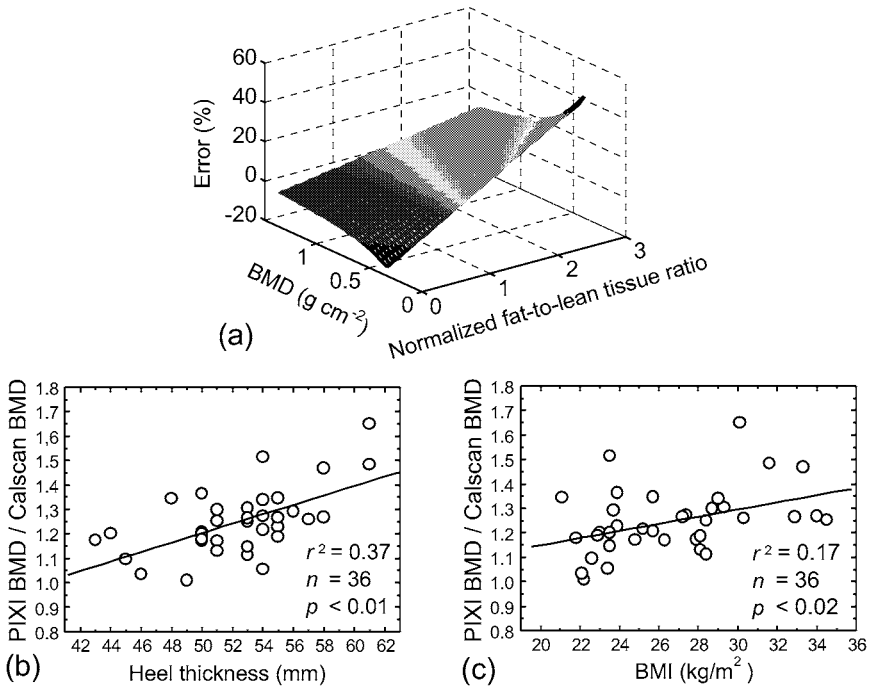

Figure 9.1: Relative error (%) in DXA- measured BMD value as a function of the true BMD values and normalized fat-to-lean tissue ratio (a). Ratio of calcaneal BMD values, as determined with Lunar PIXI and DXL Calscan, as a function of heel thickness (b) and body mass index (BMI) (c).

9.2 Site- and frequency-dependent variation of acoustic parameters

In most acoustic, mechanical and density parameters, the site-dependent variation was significant (Table 9.2). In both bovine and human trabecular bone, the topographical variations were similar with vBMD, σ_{max}, E, SOS, IRC and BUB (Table 9.2). However, only in bovine trabecular bone the topographical variations were statistically significant ($p < 0.01$, Kruskall-Wallis H test). In bovine trabecular bone,

the highest IRC and BUB values (-14.9 ± 2.0 dB and -32.2 ± 3.0 dB, respectively) were recorded in femoral caput whereas the lowest (-27.2 ± 2.0 dB and -37.3 ± 2.2 dB, respectively) values were obtained in femoral trochanter major (Table 9.2). In contrast to other parameters, nBUA showed no site-dependent variation in bovine trabecular bone.

Table 9.2: Mean values (±SD) of volumetric bone mineral density (vBMD), acoustic (at 0.5 MHz) and mechanical properties of trabecular bone in different species and different measurement sites *in vitro*.

Site	n	vBMD (g/cm^3)	nBUA (dB/MHz/cm)	SOS (m/s)	BUB (dB)	IRC (dB)	σ_{max} (MPa)	E (MPa)
Human								
FMC	8-10	0.24±0.07	80±22	2180±149	-26.0±3.4	-12.6±5.0	10.9±4.2	624±214
TMP	10	0.21±0.07	61±20	1869±393	-27.4±4.2	-13.3±4.8	9.5±3.9	575±179
FG	6	0.26±0.05	52±39	2252±59	-27.0±5.6	-13.1±4.5	-	-
Bovine								
FMC	10	0.49±0.07	40±11	1855±188	-29.9±2.2	-17.9±3.9	12.7±3.2	1024±294
FLC	10	0.38±0.07	41±18	1872±266	-31.7±3.4	-20.3±3.8	12.2±6.6	1067±794
FTM	10	0.19±0.03	40±24	1571±238	-37.3±2.2	-27.2±2.0	4.7±1.5	402±114
FC	11	0.59±0.08	32±9	2172±109	-32.2±3.0	-14.9±2.0	22.9±5.2	2085±477

In addition, spatial variation of the acoustic parameters within the ROI was revealed at all frequencies (Figure 9.2). The increase in the transducer center frequency led to an increase of 23.2% and 38.6% in the mean spatial variation of nBUA and IRC, respectively. The mean spatial variation of SOS, however, increased only slightly (from 9.9% to 23.8%) as a function of frequency (from 0.5 MHz to 5 MHz, respectively).

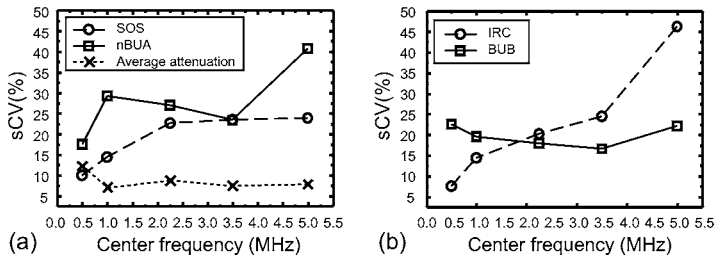

Figure 9.2: Spatial variation (sCV%) of the acoustic parameters, measured in (a) through-transmission and (b) pulse-echo geometry, as a function of transducer center frequency in human trabecular bone.

The values of quantitative ultrasound parameters were significantly dependent on frequency ($p < 0.01$, Friedman test, Figure 9.3). The average attenuation increased by 39.4 dB and nBUA decreased by 52.1 dB/MHz/cm as the transducer frequency

increased from 0.5 MHz to 5 MHz (Figure 9.3). Moreover, IRC and BUB increased (by 3.2 dB and 10.7 dB, respectively) as a function of transducer center frequency (from 0.5 MHz to 5 MHz, Figure 9.3).

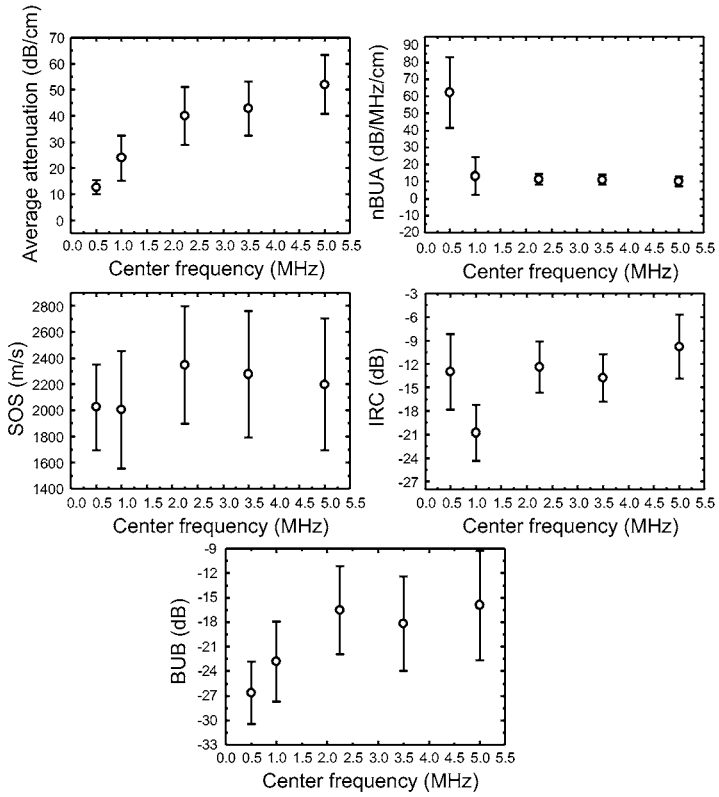

Figure 9.3: Mean values (±SD) of the acoustic parameters as a function of transducer center frequency in human trabecular bone.

9.3 Acoustic and mechanical properties of trabecular bone

Significant relationships were found between BUB or IRC and mechanical parameters in bovine ($r > 0.32$ and $r > 0.81$, $n = 41$, $p < 0.01$, respectively) and especially in human trabecular bone ($r > 0.54$ and $r > 0.70$, $n =$ 19-20, $p < 0.01$, respectively). On the other hand, in bovine trabecular bone, nBUA showed only a weak or no association ($|r| < 0.36$, $n = 41$, $p > 0.02$) with the mechanical properties. In human trabecular bone, nBUA demonstrated a significant relation ($r > 0.56$, n

=19, $p < 0.01$) with the mechanical properties only when measured at 1 MHz center frequency. In contrast to nBUA, SOS was strongly related to the mechanical properties of bovine ($r > 0.87$, $n = 41$, $p < 0.01$) and human trabecular bone ($r > 0.51$, $n = 18$, $p < 0.05$). Volumetric BMD (vBMD) exhibited a highly linear correlation ($p < 0.01$) with the mechanical properties of bovine ($r > 0.84$) and human trabecular bone ($r > 0.73$). In bovine trabecular bone, nBUA was the only parameter which demonstrated a significant correlation with the yield strain ($r = 0.31$, $n = 41$, $p < 0.05$).

The correlations between acoustic and mechanical parameters were significantly dependent on the ultrasound frequency in human bone (Figure 9.4).

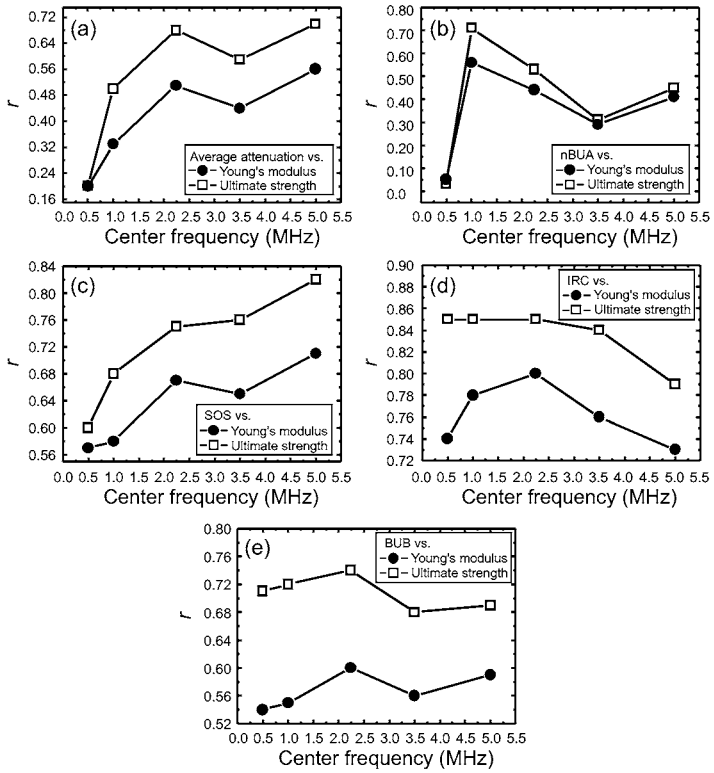

Figure 9.4: Frequency dependence of linear correlation coefficient (r) between mechanical properties and (a) average attenuation, (b) nBUA, (c) SOS, (d) IRC or (e) BUB in human trabecular bone.

The strength of association between SOS and mechanical parameters or density increased as a function of frequency (for ultimate strength: from $r = 0.60$ to $r = 0.82$, from 0.5 MHz to 5 MHz, respectively; Figure 9.4c). In contrast to SOS,

strong linear correlations between nBUA and mechanical parameters or density were found only at the center frequency of 1 MHz (for ultimate strength $r = 0.71$, $p < 0.01$, Figure 9.4b). Statistically significant moderate to strong correlations between average attenuation and mechanical parameters (for ultimate strength $r = 0.70$, $p < 0.01$, at 5 MHz, Figure 9.4a) were found at center frequencies of 2.25 MHz and 5 MHz. Only a minor variation was revealed in the linear correlations between BUB or IRC and mechanical parameters or density as a function of frequency (for ultimate strength $r = 0.74$ and $r = 0.85$ for BUB and IRC at the center frequency of 2.25 MHz, respectively, $p < 0.01$, Figure 9.4d,e).

Stepwise linear regression analyses indicated that the combination of IRC and SOS significantly improved the prediction of ultimate strength both in bovine and human trabecular bone ($r = 0.92$ and $r = 0.88$, $p < 0.01$, respectively). The ability of QUS parameters to predict ultimate strength of human trabecular bone was further improved ($r = 0.93$, $p < 0.01$) when BUB was combined with IRC and SOS. No other combination of ultrasound parameters could improve ($p > 0.05$) the prediction of the mechanical parameters. On the other hand, the combination of SOS and IRC improved significantly the prediction of vBMD in human trabecular bone with center frequencies of 0.5 MHz and 5 MHz ($r = 0.81$ and $r = 0.89$, $p < 0.01$, respectively).

9.4 QUS assessment of trabecular bone microstructure

The human trabecular bone samples were highly porous, with the mean trabecular bone volume fraction (BV/TV) of 17.1%. Furthermore, considerable variation (range) was observed in trabecular spacing (Tb.Sp., 482-947 μm), structural model index (SMI, 0.27-1.52), connectivity (2.9-13.6 mm^{-3}) and bone surface-to-volume ratio (BS/BV, 13.8-24.8 mm^{-1}) (Table 9.3). Trabecular thickness values ranged from 152 μm to 264 μm (Table 9.3).

Table 9.3: Mean values, standard deviations (SD), maximum (Max) and minimum (Min) values of microstructural parameters of human trabecular bone ($n = 26$) *in vitro*.

Parameter	Mean	SD	Max	Min
BV/TV (%)	17.1	4.2	25.7	9.4
Tb.Th. (μm)	199	28	264	152
Tb.Sp. (μm)	719	110	947	482
SMI (-)	0.87	0.31	1.52	0.27
BS/BV (mm^{-1})	18.4	2.6	24.8	13.8
Connectivity (mm^{-3})	5.99	2.45	13.6	2.9

The association between the structural and acoustic parameters was investigated using Pearson's correlation analysis. The strongest correlations between SOS and structural parameters were typically found with the center frequency of 5 MHz (Figure 9.5c). The correlation coefficient between SOS and trabecular spacing was $r = -0.38$ ($p > 0.05$) and $r = -0.62$ ($p < 0.01$) at center frequencies of 0.5 MHz and

5 MHz, respectively (Figure 9.5c). In contrast to SOS, the strongest associations between nBUA or average attenuation and structural parameters were found, in general, at center frequencies of 1 MHz and 2.25 MHz (r = 0.37-0.84 and r = -0.13- -0.70 for average attenuation and nBUA at center frequency of 2.25 MHz, respectively; Figure 9.5a,b). At all ultrasound frequencies, the relationships between structural parameters (except Tb.Sp. and connectivity at 0.5 MHz) and BUB or IRC were significant (Figure 9.5d,e). At the center frequency of 1 MHz, the association between the acoustic parameters and the BV/TV was strong (r = 0.70-0.84, $p <$ 0.01).

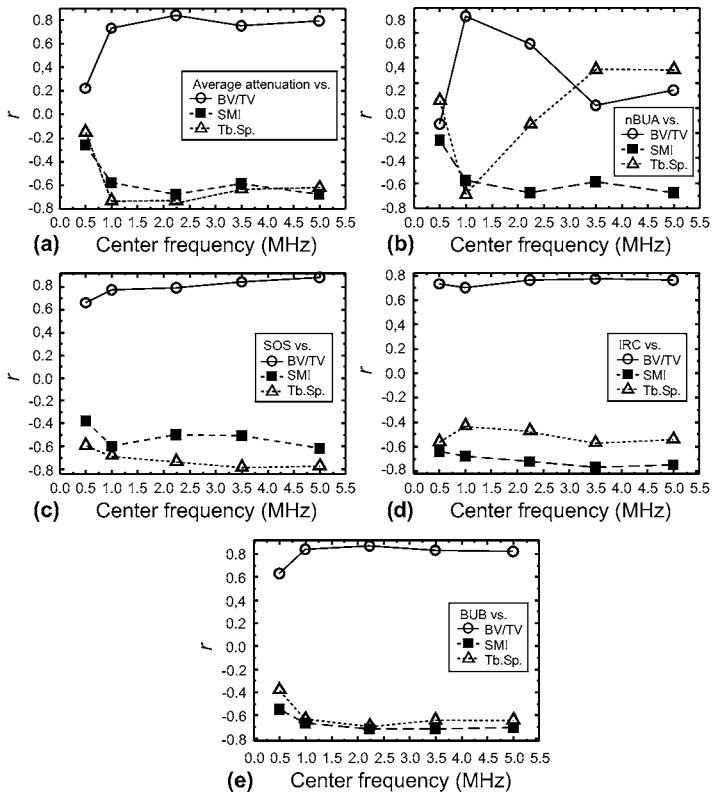

Figure 9.5: Frequency dependence of the strength of correlations (r) between the structural parameters and (a) average attenuation, (b) nBUA, (c) SOS, (d) IRC or (e) BUB and structural parameters as a function of transducer center frequency in human trabecular bone.

Three independent structural components were obtained from the principal component analyses: 1) trabecular structure, 2) surface and 3) anisotropy component

(for details, see Study IV (Table 3)). BUB showed the strongest correlations (r = -0.40- -0.67, $p < 0.05$) with the trabecular structure component at all frequencies whereas the strongest association (r = -0.59, $p < 0.01$) between IRC and the trabecular structure component was only revealed at high frequencies (>2.25 MHz). With most acoustic parameters (average attenuation, nBUA, IRC and BUB), the strength of correlations with structural components was related to frequency. The anisotropy component showed no association with any of the acoustic parameters ($r < 0.31$, $p > 0.05$).

At the center frequency of 1 MHz, BV/TV remained the primary determinant of the nBUA, average attenuation and BUB (r^2 = 0.53-0.70, $p < 0.01$, stepwise linear regression analysis, Table 9.4). In addition, DA contributed significantly to the nBUA, with the average attenuation and BUB explaining an additional 9-10% of the variance in these parameters ($p < 0.05$, Table 9.4). Furthermore, DA improved significantly the prediction of average attenuation at the center frequency of 3.5 MHz, explaining an additional 12% of variation ($p < 0.05$, Table 9.4). At all ultrasound frequencies (with the exception of 1 MHz), BV/TV was the strongest determinant of the SOS. At the center frequency of 2.25 MHz, BS/BV and Tb.Sp. contributed significantly to the prediction of SOS, accounting for an additional 12% of the variation ($p < 0.05$, Table 9.4).

Table 9.4: Multivariate linear regression analysis (r^2, $p < 0.05$) between the structural parameters and acoustic properties at different frequencies. The improvement of linear correlation (Δr^2), as compared to the simple linear regression, is also shown.

Dependent variable	Independent variables	r^2	Δr^2
1 MHz:			
nBUA	BV/TV, DA	0.63	0.09
Average attenuation	BV/TV, DA	0.63	0.10
BUB	BV/TV, DA	0.80	0.10
2.25 MHz:			
SOS	BV/TV, BS/BV	0.68	0.06
SOS	BV/TV, BS/BV, Tb.Sp.	0.77	0.09
SOS	BS/BV, Tb.Sp.	0.74	-0.03
3.5 MHz:			
nBUA	Tb.Th., connectivity	0.39	0.12
Average attenuation	BV/TV, DA	0.68	0.12
5 MHz:			
nBUA	BS/BV, Tb.Sp.	0.40	0.12

Numerically and experimentally determined SOS and average attenuation values were strongly interrelated ($r = 0.86$ and $r = 0.89$, $p < 0.01$, respectively). Moreover, the differences between the parameter values extracted from numerical simulations and experimental measurements were minor (SOS: 2197 ± 323 m/s and 2207 ± 500 m/s, average attenuation: 40.5 ± 12.0 dB/cm and 38.0 ± 13.1 dB/cm, respectively).

Chapter X
Discussion

In the present study, relationships between the density, acoustic, mechanical and structural properties of trabecular bone were investigated. Initially, the reproducibilities of the acoustic parameters and the relationships between the acoustic and mechanical parameters were evaluated in bovine trabecular bone. This was done to reveal the advantages and feasibility of the ultrasound, particularly backscattering techniques to predict bone characteristics. Subsequently, the acoustic measurements were conducted over a wide frequency range using spatial scanning to understand the role of spatial averaging and to determine the most sensitive frequency for assessment of the mechanical and structural properties of human trabecular bone. In addition, inaccuracies were explored in the DXA technique which is used for osteoporosis risk evaluation. Furthermore, a recently developed technique, dual energy X-ray laser, was evaluated and the performance of the device was assessed.

Dual energy X-ray laser technique

The technical performance of a clinical instrument is characterized by its precision and accuracy. In Study I, the precision of DXL Calscan was found to be similar to that of calcaneal DXA instruments [122, 140, 73]. Although the accuracy was not investigated in Study I, previous studies have demonstrated, both *in vitro* and *in vivo*, that the accuracy of DXL Calscan is similar to or even better than that of axial DXA or QUS devices [149, 85, 148]. The combination of DXA and laser measurements may diminish the precision of the technique due to the inherent inaccuracies related to each measurement. However, the present and earlier studies [85] demonstrated the good *in vivo* precision with the DXL Calscan instrument.

The demand for reliable osteoporosis diagnosis and monitoring sets high requirements for clinical instruments. In clinical DXA measurements of BMD, significant errors up to 0.1 g/cm^2 [153] (approximately equal to $\pm$ 1 T-score [95]) may occur. Such a large error can lead to a diagnostic misinterpretation [12]. Especially in cases of longitudinal monitoring, changes in soft tissue composition can compromise the

reliability of the diagnosis [94, 126, 129, 152, 153]. The differences between BMD values measured with DXL Calscan and Lunar PIXI were positively related to heel thickness and BMI, thus indicating that in the DXL and DXA techniques, the soft tissue correction is different. In contrast to the standard two-component DXA technique, the DXL technique includes a determination of heel thickness which may reduce the error attributable to the soft tissue on the measured BMD.

Quantitative ultrasound measurements

In Study II, the reproducibilities of the backscattering parameters were slightly lower that those of clinical QUS parameters (BUA and SOS). The difference may be explained, as suggested earlier, by the more complex data acquisition and signal processing methods involved [134] and also by a lack of spatial averaging of the measurements (Study II).

In the present study, the values of acoustic and mechanical properties of bovine trabecular bone and structural parameters of human trabecular bone were in good agreement with the previous studies [61, 138, 158, 31, 127]. The differences between the results of the present study and earlier studies may be explained by the natural variation between the collected samples and differences in the analysis methods and measuring techniques.

QUS and microstructure of trabecular bone

In human trabecular bone, the relationships between the QUS parameters and microstructural characteristics were significant, although frequency dependent. The negative association between SMI and QUS parameters indicates that the increase of velocity, attenuation and scattering are associated with a more plate-like shape of the trabeculae. Earlier, Nicholson *et al* [108] found a similar association in calcaneus. The multiple regression analyses revealed that the bone volume fraction was the strongest determinant of the variation occurring in the acoustic parameters. Nevertheless, other structural parameters, such as DA, BS/BV, Tb.Sp. and connectivity, were also significantly related to the acoustic parameters. In addition, principal component analysis was applied. Interestingly, the strongest determinants of BUB were the structural variables reflecting the trabecular characteristics. In particular, the variation in trabecular properties not related to the surface characteristics was found to affect the BUB to a significant degree. On the other hand, IRC showed a similar trend only at high frequencies (>2.25 MHz) while at lower frequencies, the most significant association was found with the surface component.

QUS and mechanical properties of trabecular bone

SOS showed significant correlations with the density and mechanical parameters at

all frequencies in human and bovine trabecular bone. In contrast to SOS, nBUA demonstrated a non-significant correlation with the density or the mechanical properties of bovine trabecular bone, as found earlier also by others [157]. In human trabecular bone, a significant association between nBUA and density or mechanical properties was found only at specific frequencies. These findings suggest that nBUA can predict mechanical properties of trabecular bone at certain densities, frequencies and measurement sites. IRC is, at least theoretically, dependent on the difference in the acoustic impedance between the bone and the coupling medium. Thus, it is related to the density and elastic modulus of the trabecular bone framework. In addition, the association of ultrasound backscattering with trabecular bone density [167, 23] (Studies II and III), microstructure [23] (Study IV), anisotropy [167] and collagen [63] or bone marrow contents [106] suggests that the backscattering measurements may be used for the assessment of the density, structure and composition of trabecular bone. On the other hand, it has been demonstrated that the mechanical properties of trabecular bone are strongly related to density [21], the structure of the trabecular bone [180] and the composition of the organic matrix [18]. In the light of these results, one might hypothesize that the ultrasound reflection and backscattering are also related to the mechanical properties. In the present study, this was indeed observed both in bovine and human trabecular bone; IRC and BUB showed consistent significant associations with density or mechanical parameters in bovine trabecular bone and especially in human trabecular bone.

Frequency dependence of QUS parameters

In Studies III and IV, the frequency dependence of acoustic parameters was found to be significant ($p < 0.01$). Frequency-dependent attenuation and dispersion may alter the spectral characteristics of the waveform and, thus affect the determination of TOF [168]. This could explain the frequency dependence of SOS seen in Studies III and IV. In line with the existing literature [90], at high frequencies, nBUA values were lower than those of measured at low frequencies. Average attenuation, as expected, increased as a function of frequency. Interestingly, a minor nonsystematic increase was revealed also with IRC values. Since reflection is not frequency dependent, this variation may be due to the improved spatial resolution (smaller beam diameter) at high frequencies. In addition, in a highly porous medium such as trabecular bone and at wavelengths comparable to the pore size, IRC may be influenced by scattering processes. BUB was found to increase as a function of frequency. Although extensive theoretical and experimental research on frequency-dependent backscattering [24, 74, 110, 133, 166, 169] has been conducted, our understanding about the backscattering phenomenon in trabecular bone is still limited.

The strengths of relationships between the measured acoustic and mechanical or structural parameters were dependent on the frequency (Studies III and IV). As the heterogeneity of trabecular bone microstructure leads to a significant variation in

elastic modulus and strength within the measurement site [17, 48], spatial averaging, ultrasound focusing and frequency play important roles in the acoustic evaluation of the mechanical and structural properties of trabecular bone. Higher frequencies provide improved axial and spatial resolution which would be expected to influence the relationships between the acoustic and the structural or mechanical parameters. In the present study, SOS exhibited a significant correlation with the density, mechanical and structural properties at all frequencies, showing the strongest associations at 5 MHz. Since higher frequencies possess smaller wavelengths, the determination of TOF becomes more accurate as the frequency increases. Consequently, due to the improved axial accuracy, SOS values measured at higher frequencies may provide a better estimate of the density, mechanical and structural properties of trabecular bone as found in the present study. For average attenuation, nBUA, IRC and BUB, the association with the structural and mechanical properties was strongest at lower frequencies (within range from 1 MHz to 3.5 MHz). However, the association between IRC or BUB and structural characteristics was not consistent across different frequencies. Wear [169] revealed a significant increase in the backscatter coefficient at >2 MHz for scatterer sizes of 200-300 μm. These findings are further supported by an earlier theoretical investigation [35]. In Study IV, the mean trabecular thickness of the samples was 199 $\pm$ 28 μm. The mean trabecular spacing measured in Study IV (719 $\pm$ 110 μm) corresponds to the scatterer spacing (800 μm) used by Wear [169]. Therefore, the frequency dependence in the strength of association between backscattering and microstructure observed in Study IV appears to be typical of the scattering phenomenon in porous materials. Since different skeletal sites possess different microstructures, the selection of optimal frequency range may have to be considered site-specifically. Interestingly, the strength of the association between the acoustic and the mechanical or structural properties was more frequency dependent with the parameters measured using through-transmission technique than those determined using the pulse-echo technique.

Potential of pulse-echo ultrasound

Although SOS was a good predictor of mechanical and structural properties of bovine and human trabecular bone, its clinical feasibility may be impaired as it cannot be measured *in vivo* using a single transducer, if there is no information available about the bone thickness. BUB and IRC can be determined *in vivo* with a pulse-echo technique using only one transducer. In principle, this enables assessment of the bone status at skeletal sites which cannot be easily accessed from both sides (*e.g.* proximal femur). As suggested earlier [23, 63, 134], the direct measurement of acoustic parameters at potential fracture sites such as a hip or a wrist would be anticipated to improve the diagnostic capability of quantitative ultrasound techniques.

Summary

In summary, clinical DXA measurements (BMD) are affected by variations in the compositions of soft tissue and bone marrow. The changes in soft tissue thickness and composition can lead to significant uncertainty in the BMD results, as demonstrated by the present numerical simulations. Based on the current investigation, the DXL Calscan provides an equally precise measure of calcaneal BMD as can be achieved with the traditional DXA devices.

The present study suggests that while 0.5 MHz is the most commonly used frequency in clinical bone ultrasound measurements, the higher frequencies may provide additional information on density, mechanical and structural properties of trabecular bone, information which is not attainable at lower frequencies. Nevertheless, the high attenuation in human trabecular bone limits the frequency bandwidth available for measurements. In clinical applications, the soft tissue and cortical bone overlying the trabecular bone affect the acoustic measurements. These sources of interference must be considered and eliminated/minimized prior to *in vivo* measurements. Numerous correction methods have been introduced for the artefacts attributable to soft tissue in ultrasound measurements [20, 67, 98]. Possibly, some of these methods can be adapted for the acoustic measurement of trabecular bone. The cortical layer may strongly govern the *in vivo* strength of the whole bone [93] and ultrasonic measurements of cortical bone thickness and acoustic properties may yield useful information on bone strength and fracture risk [2]. Based on the present results, it is concluded that the ultrasound backscattering measurement may have clinical potential and that the selection of optimal frequency for QUS measurement, *e.g.* depending on the anatomical site of the measurement, plays an important role in the assessment of bone status.

CHAPTER XI

Summary and conclusions

Quantitative ultrasound techniques are potential tools for use in osteoporosis screening. Further improvements in QUS analyses and measurement techniques are still needed to increase the feasibility of using these techniques.

The present study characterized dual energy X-ray laser (DXL) and ultrasound backscattering techniques. In particular, the relationships between QUS parameters and density, mechanical or structural properties of trabecular bone were studied. In addition, one aim of the present study was to compare ultrasound transmission and backscattering parameters and to determine the most sensitive frequency range for the assessment of trabecular bone status.

The most important results can be summarized as follows:

- The DXL technique provides a reproducible method for the measurement of calcaneal BMD.
- In calcaneal BMD measurements, the DXL technique provides a correction for soft tissue effects that is different from that used in the traditional DXA technique.
- QUS at 2.25 MHz and at higher center frequencies was found to be sensitive to variations in density, mechanical and structural properties of the human femoral and tibial trabecular bone.
- BUB and IRC are strong predictors of the density, mechanical and structural properties of trabecular bone. In contrast to BUA and SOS, backscattering measurements may be used to assess bone quality at typical fracture sites.

[1] Aloia J. F., Vaswani A., Ma R., and Flaster E. Comparative study of body composition by dual-energy x-ray absorptiometry. *J Nucl Med*, 36(8):1392–1397, 1995.

[2] Augat P., Iida H., Jiang Y., Diao E., and Genant H. K. Distal radius fractures: mechanisms of injury and strength prediction by bone mineral assessment. *J Orthop Res*, 16(5):629–635, 1998.

[3] Bailey A. J., Wotton S. F., Sims T. J., and Thompson P. W. Post-translational modifications in the collagen of human osteoporotic femoral head. *Biochem Biophys Res Commun*, 185(3):801–805, 1992.

[4] Bauer D. C., Gluer C. C., Cauley J. A., Vogt T. M., Ensrud K. E., Genant H. K., and Black D. M. Broadband ultrasound attenuation predicts fractures strongly and independently of densitometry in older women. A prospective study. Study of Osteoporotic Fractures Research Group. *Arch Intern Med*, 157(6):629–634, 1997.

[5] Biot M. A. Theory of propagation of elastic waves in a fluid saturated porous solid i. Low frequency range. *J Acoust Soc Am*, 28:168–178, 1956.

[6] Black D. M., Cummings S. R., Genant H. K., Nevitt M. C., Palermo L., and Browner W. Axial and appendicular bone density predict fractures in older women. *J Bone Miner Res*, 7(6):633–638, 1992.

[7] Blake G. M., Wahner H. W., and Fogelman I. *The evaluation of osteoporosis: Dual energy X-ray absorptiometry and ultrasound in clinical practise.* Martin Dunitz Ltd, London, 2nd edition, 1999.

[8] Bland J. M. and Altman D. G. Statistical methods for assessing agreement between two methods of clinical measurement. *Lancet*, 1(8476):307–310, 1986.

[9] Bloom W and Fawcett D. W. *A Textbook of Histology.* W. B. Saunders Comp, Philadelphia, 9th edition, 1970.

[10] Bolotin H. H. Analytic and quantitative exposition of patient-specific systematic inaccuracies inherent in planar dxa-derived in vivo BMD measurements. *Med Phys*, 25(2):139–151, 1998.

[11] Bolotin H. H. A new perspective on the causal influence of soft tissue composition on DXA-measured in vivo bone mineral density. *J Bone Miner Res*, 13(11):1739–1746,

1998.

[12] Bolotin H. H. and Sievanen H. Inaccuracies inherent in dual-energy x-ray absorptiometry in vivo bone mineral density can seriously mislead diagnostic/prognostic interpretations of patient-specific bone fragility. *J Bone Miner Res*, 16(5):799–805, 2001.

[13] Bolotin H. H., Sievanen H., Grashuis J. L., Kuiper J. W., and N. Järvinen T. L. Inaccuracies inherent in patient-specific dual-energy x-ray absorptiometry bone mineral density measurements: comprehensive phantom-based evaluation. *J Bone Miner Res*, 16(2):417–426, 2001.

[14] Boutry N., Cortet B., Dubois P., Marchandise X., and Cotten A. Trabecular bone structure of the calcaneus: preliminary in vivo MR imaging assessment in men with osteoporosis. *Radiology*, 227(3):708–717, 2003.

[15] Bowen T., Connor W. G., Nasoni R. L., Pifer A. E., and Sholes R. R. Measurement of the temperature dependence of the velocity of ultrasound in soft tissues. In Kinzer M., editor, *Ultrasound Tissue Characterization II (National Bureau of Standards Special Publication 525)*, pages 57–61. US Goverment, Washington DC, 1979.

[16] Braun M. J., Meta M. D., Schneider P., and Reiners C. Clinical evaluation of a high-resolution new peripheral quantitative computerized tomography (pQCT) scanner for the bone densitometry at the lower limbs. *Phys Med Biol*, 43(8):2279–2294, 1998.

[17] Brown T. D. and Ferguson Jr., A. B. Mechanical property distributions in the cancellous bone of the human proximal femur. *Acta Orthop Scand*, 51(3):429–437, 1980.

[18] Burr D.B. The contribution of the organic matrix to bone's material properties. *Bone*, 31(1):8–11, 2002.

[19] Cadossi R. and Cane V. Pathways of transmission of ultrasound energy through the distal metaphysis of the second phalanx of pigs: an in vitro study. *Osteoporos Int*, 6(3):196–206, 1996.

[20] Carpenter D. A., Kossoff G., and Griffiths K. A. Correction of distortion in US images caused by subcutaneous tissues: results in tissue phantoms and human subjects. *Radiology*, 195(2):563–567, 1995.

[21] Carter D. R. and Hayes W. C. The compressive behavior of bone as a two-phase porous structure. *J Bone Joint Surg Am*, 59(7):954–962, 1977.

[22] Cendre E., Kaftandjian V., Peix G., Jourlin M., Mitton D., and Babot D. An investigation of segmentation methods and texture analysis applied to tomographic images of human vertebral cancellous bone. *J Microsc*, 197 (Pt 3):305–316, 2000.

[23] Chaffaî S., Peyrin F., Nuzzo S., Porcher R., Berger G., and Laugier P. Ultrasonic characterization of human cancellous bone using transmission and backscatter measurements: Relationship to density and microstructure. *Bone*, 30(1):229–236, 2002.

[24] Chaffaî S., Roberjot V., Peyrin F., Berger G., and Laugier P. Frequency dependence of ultrasonic backscattering in cancellous bone: autocorrelation model and experimental results. *J Acoust Soc Am*, 108(5 Pt 1):2403–2411, 2000.

[25] Chenevert T. L., Bylski D. I., Carson P. L., Meyer C. R., Bland P. H., Adler D. D.,

and Schmitt R. M. Ultrasonic computed tomography of the breast. Improvement of image quality by use of cross-correlation time-of-flight and phase-insensitive attenuation measurements. *Radiology*, 152(1):155–159, 1984.

[26] Cheng S., Tylavsky F. A., Orwoll E. S., Rho J. Y., and Carbone L. D. The role of collagen abnormalities in ultrasound and densitometry assessment: In vivo evidence. *Calcif Tissue Int*, 64(6):470–476, 1999.

[27] Chérin E., Saïed A., Laugier P., Netter P., and Berger G. Evaluation of acoustical parameter sensitivity to age-related and osteoarthritic changes in articular cartilage using 50-MHz ultrasound. *Ultrasound Med Biol*, 24(3):341–354, 1998.

[28] Cortet B., Boutry N., Dubois P., Legroux-Gerot I., Cotten A., and Marchandise X. Does quantitative ultrasound of bone reflect more bone mineral density than bone microarchitecture? *Calcif Tissue Int*, 74(1):60–67, 2004.

[29] Ding M., Day J. S., Burr D. B., Mashiba T., Hirano T., Weinans H., Sumner D. R., and Hvid I. Canine cancellous bone microarchitecture after one year of high-dose biphosphonates. *Calcif Tissue Int*, 72:737–744, 2003.

[30] Ding M., Odgaard A., and Hvid I. Accuracy of cancellous bone volume fraction measured by micro-CT scanning. *J Biomech*, 32(3):323–326, 1999.

[31] Ding M., Odgaard A., and Hvid I. Changes in the three-dimensional microstructure of human tibial cancellous bone in early osteoarthritis. *J Bone Joint Surg Br*, 85(6):906–912, 2003.

[32] Düppe H., Gardsell P., Nilsson B., and Johnell O. A single bone density measurement can predict fractures over 25 years. *Calcif Tissue Int*, 60(2):171–174, 1997.

[33] Drozdzowska B., Pluskiewicz W., and Przedlacki J. Prediction of the biomechanical properties of cancellous bone using ultrasound velocity and bone mineral density - an in vitro study. *Med Sci Monit*, 8:MT15–MT20, 2002.

[34] Economos C. D., Nelson M. E., Fiatarone Singh M. A., Kehayias J. J., Dallal G. E., Heymsfield S. B., Wang J., Yasumura S., Ma R., and Pierson Jr., R. N. Bone mineral measurements: a comparison of delayed gamma neutron activation, dual-energy x-ray absorptiometry and direct chemical analysis. *Osteoporos Int*, 10(3):200–206, 1999.

[35] Faran J. J. Jr. Sound scattering by solid cylinders and spheres. *J Acoust Soc Am*, 23(4):405–419, 1951.

[36] Feldkamp L. A., Goldstein S. A., Parfitt A. M., Jesion G., and Kleerekoper M. The direct examination of three-dimensional bone architecture in vitro by computed tomography. *J Bone Miner Res*, 4(1):3–11, 1989.

[37] Feldkamp L. A. and Jesion G. 3-d x-ray computed tomography. In Thompson S. O. and Chimenti D. E., editors, *Review of progress in quantitative non-destructive evaluation*, pages 555–566. Plenum, New York, 1986.

[38] Formica C., Loro M. L., Gilsanz V., and Seeman E. Inhomogeneity in body fat distribution may result in inaccuracy in the measurement of vertebral bone mass. *J Bone Miner Res*, 10(10):1504–1511, 1995.

[39] Frost M. L., Blake G. M., and Fogelman I. Quantitative ultrasound and bone mineral density are equally strongly associated with risk factors for osteoporosis. *J*

Bone Miner Res, 16(2):406–416, 2001.

[40] Frucht A. H. Die schallgeschwindigkeit in menschlichen und tierischen geweben. *Z ges exp Med*, 120:526–557, 1953.

[41] Fry F. J. and Barger J. E. Acoustical properties of the human skull. *J Acoust Soc Am*, 63(5):1576–1590, 1978.

[42] Gartner L. P and Hiatt J. L. *Color Textbook of Histology*. W.B. Saunders Comp., Philadelphia, 2nd edition, 2001.

[43] Giesen E. B. W., Ding M., Dalstra M., and van Eijden T. M. G. J. Architectural measures of the cancellous bone of the mandibular condyle identified by principal components analysis. *Calcif Tissue Int*, 73:225–231, 2003.

[44] Glüer C. C., Blake G., Lu Y., Blunt B. A., Jergas M., and Genant H. K. Accurate assessment of precision errors: how to measure the reproducibility of bone densitometry techniques. *Osteoporos Int*, 5(4):262–270, 1995.

[45] Glüer C. C., Cummings S. R., Bauer D. C., Stone K., Pressman A., Mathur A., and Genant H. K. Osteoporosis: association of recent fractures with quantitative US findings. *Radiology*, 199(3):725–732, 1996.

[46] Glüer C. C., Wu C. Y., Jergas M., Goldstein S. A., and Genant H. K. Three quantitative ultrasound parameters reflect bone structure. *Calcif Tissue Int*, 55(1):46–52, 1994.

[47] Goldman D. E. and Richards J. R. Measurement of high-frequency sound velocity in mammalian soft tissues. *J Acoust Soc Am*, 26:981–983, 1954.

[48] Goldstein S. A., Wilson D. L., Sonstegard D. A., and Matthews L. S. The mechanical properties of human tibial trabecular bone as a function of metaphyseal location. *J Biomech*, 16(12):965–969, 1983.

[49] Goulet R. W., Goldstein S. A., Ciarelli M. J., Kuhn J. L., Brown M. B., and Feldkamp L. A. The relationship between the structural and orthogonal compressive properties of trabecular bone. *J Biomech*, 27(4):375–389, 1994.

[50] Greenleaf J. F., Johnson S. A., Samayoa W. F., and Duck F. A. Two-dimensional acoustic velocity distributions in tissues using an algebraic reconstruction technique. In *Ultrasound International Conference Proceedings*, pages 190–194, London, UK, 1975. Guilford, UK: IPC Science and Technology Press.

[51] Grimm M. J. and Williams J. L. Assessment of bone quantity and 'quality' by ultrasound attenuation and velocity in the heel. *Clin Biomech*, 12(5):281–285, 1997.

[52] Hangartner T. N. and Johnston C. C. Influence of fat on bone measurements with dual-energy absorptiometry. *Bone Miner*, 9(1):71–81, 1990.

[53] Hans D., Dargent-Molina P., Schott A. M., Sebert J. L., Cormier C., Kotzki P. O., Delmas P. D., Pouilles J. M., Breart G., and Meunier P. J. Ultrasonographic heel measurements to predict hip fracture in elderly women: the EPIDOS prospective study. *Lancet*, 348(9026):511–514, 1996.

[54] Hans D., Wu C., Njeh C. F., Zhao S., Augat P., Newitt D., Link T., Lu Y., Majumdar S., and Genant H. K. Ultrasound velocity of trabecular cubes reflects mainly bone density and elasticity. *Calcif Tissue Int*, 64:18–23, 1999.

[55] Hara T., Tanck E., Homminga J., and Huiskes R. The influence of microcomputed

tomography threshold variations on the assessment of structural and mechanical trabecular bone properties. *Bone*, 31(1):107–109, 2002.

[56] Harrigan T. P. and Mann R. W. Characterization of microstructural anisotropy in orthotropic materials using a second rank tensor. *J Mater Sci*, 19:761–767, 1984.

[57] Haworth C. S., Selby P. L., Adams J. E., Mawer E. B., Horrocks A. W., and Webb A. K. Effect of intravenous pamidronate on bone mineral density in adults with cystic fibrosis. *Thorax*, 56(4):314–316, 2001.

[58] Hildebrand T. and Ruegsegger P. A new method for the model-independent assessment of thickness in three-dimensional images. *J Microsc*, 185:67–75, 1997.

[59] Hildebrand T. and Ruegsegger P. Quantification of bone microarchitecture with the structure model index. *Comput Methods Biomech Biomed Engin*, 1(1):15–23, 1997.

[60] Hodgskinson R. and Currey J. D. The effect of variation in structure on the Young's modulus of cancellous bone: a comparison of human and non-human material. *Proc Inst Mech Eng*, 204(2):115–121, 1990.

[61] Hodgskinson R., Njeh C. F., Currey J. D., and Langton C. M. The ability of ultrasound velocity to predict the stiffness of cancellous bone in vitro. *Bone*, 21(2):183–190, 1997.

[62] Hodgskinson R., Njeh C. F., Whitehead M. A., and Langton C. M. The non-linear relationship between BUA and porosity in cancellous bone. *Phys Med Biol*, 41(11):2411–2420, 1996.

[63] Hoffmeister B. K., Whitten S. A., Kaste S. C., and Rho J. Y. Effect of collagen and mineral content on the high-frequency ultrasonic properties of human cancellous bone. *Osteoporos Int*, 13(1):26–32, 2002.

[64] Hoffmeister B. K., Whitten S. A., and Rho J. Y. Low-megahertz ultrasonic properties of bovine cancellous bone. *Bone*, 26(6):635–642, 2000.

[65] Homminga J., Van-Rietbergen B., Lochmuller E. M., Weinans H., Eckstein F., and Huiskes R. The osteoporotic vertebral structure is well adapted to the loads of daily life, but not to infrequent "error" loads. *Bone*, 34(3):510–516, 2004.

[66] Hudelmaier M., Kollstedt A., Lochmuller E. M., Kuhn V., Eckstein F., and Link T. M. Gender differences in trabecular bone architecture of the distal radius assessed with magnetic resonance imaging and implications for mechanical competence. *Osteoporos Int*, 16(9):1124–1133, 2005.

[67] Hughes D. I. and Duck F. A. Automatic attenuation compensation for ultrasonic imaging. *Ultrasound Med Biol*, 23(5):651–664, 1997.

[68] Hvid I. Cancellous bone at the knee: a comparison of two methods of strength measurement. *Arch Orthop Trauma Surg*, 104(4):211–217, 1985.

[69] Hvid I., Bentzen S. M., Linde F., Mosekilde L., and Pongsoipetch B. X-ray quantitative computed tomography: the relations to physical properties of proximal tibial trabecular bone specimens. *J Biomech*, 22(8-9):837–844, 1989.

[70] Hvid I. and Jensen J. Cancellous bone strength at the proximal human tibia. *Eng Med*, 13(1):21–25, 1984.

[71] Hvid I., Jensen N. C., Bunger C., Solund K., and Djurhuus J. C. Bone mineral assay: its relation to the mechanical strength of cancellous bone. *Eng Med*, 14(2):79–83,

1985.

[72] Ito M., Nakamura T., Matsumoto T., Tsurusaki K., and Hayashi K. Analysis of trabecular microarchitecture of human iliac bone using microcomputed tomography in patients with hip arthrosis with or without vertebral fracture. *Bone*, 23(2):163–169, 1998.

[73] Ito M., Nishida A., Kono J., Kono M., Uetani M., and Hayashi K. Which bone densitometry and which skeletal site are clinically useful for monitoring bone mass? *Osteoporos Int*, 14(12):959–964, 2003.

[74] Jenson F., Padilla F., and Laugier P. Prediction of frequency-dependent ultrasonic backscatter in cancellous bone using statistical weak scattering model. *Ultrasound Med Biol*, 29(3):455–464, 2003.

[75] Jinnai H., Watashiba H., Kajihara T., Nishikawa Y., Takahashi M., and Ito M. Surface curvatures of trabecular bone microacrhitecture. *Bone*, 30:191–194, 2002.

[76] Jonson R. Mass attenuation coefficients, quantities and units for use in bone mineral determinations. *Osteoporos Int*, 3(2):103–106, 1993.

[77] Jonson R., Mansson L. G., Rundgren A., and Szucs J. Dual-photon absorptiometry for determination of bone mineral content in the calcaneus with correction for fat. *Phys Med Biol*, 35(7):961–969., 1990.

[78] Joseph D., Gu W. Y., mao X. G., Lai W. M., and Mow V. C. True density of normal and enzymatically treated bovine articular cartilage. In *Trans Orthop Res Soc*, volume 24, page 642, Anaheim, 1999.

[79] Joyet G., Baudraz A., and Joyet M. L. Determination of the electronic density and the average atomic number of tissues in man by gamma-ray attenuation. *Experientia*, 30(11):1338–1341, 1974.

[80] Kaye G. W. C. and Laby T. H. *Tables of Physical and Chemical Constants*, volume 12th edition. Longmans, Green and Co Ltd, London, 1959.

[81] Keaveny T. M., Wachtel E. F., Ford C. M., and Hayes W. C. Differences between the tensile and compressive strengths of bovine tibial trabecular bone depend on modulus. *J Biomech*, 27(9):1137–1146, 1994.

[82] Kinney J. H., Haupt D. L., Balooch M., Ladd A. J., Ryaby J. T., and Lane N. E. Three-dimensional morphometry of the l6 vertebra in the ovariectomized rat model of osteoporosis: biomechanical implications. *J Bone Miner Res*, 15(10):1981–1991, 2000.

[83] Kivirikko K. I. Collagens and their abnormalities in a wide spectrum of diseases. *Ann Med*, 25(2):113–126, 1993.

[84] Kuhn J. L., Goldstein S. A., Feldkamp L. A., Goulet R. W., and Jesion G. Evaluation of a microcomputed tomography system to study trabecular bone structure. *J Orthop Res*, 8(6):833–842, 1990.

[85] Kullenberg R. A new accurate technology for the determination of bone mineral areal density - dual x-ray and laser (DXL). In *Proc. 5th Int. Symp. on Clinical Advances in Osteoporosis*, Honolulu, HA, 2002.

[86] Lang T., Takada M., Gee R., Wu C., Li J., Hayashi-Clark C., Schoen S., March V., and Genant H. K. A preliminary evaluation of the lunar expert-XL for bone

densitometry and vertebral morphometry. *J Bone Miner Res*, 12(1):136–143, 1997.

[87] Langton C. M., Njeh C. F., Hodgskinson R., and Currey J. D. Prediction of mechanical properties of the human calcaneus by broadband ultrasonic attenuation. *Bone*, 18(6):495–503, 1996.

[88] Langton C. M., Palmer S. B., and Porter R. W. The measurement of broadband ultrasonic attenuation in cancellous bone. *Eng Med*, 13(2):89–91, 1984.

[89] Laugier P., Droin P., Laval-Jeantet A. M., and Berger G. In vitro assessment of the relationship between acoustic properties and bone mass density of the calcaneus by comparison of ultrasound parametric imaging and quantitative computed tomography. *Bone*, 20(2):157–165, 1997.

[90] Lee K. I., Roh H. S., and Yoon S. W. Correlations between acoustic properties and bone density in bovine cancellous bone from 0.5 to 2 MHz. *J Acoust Soc Am*, 113(5):2933–2938, 2003.

[91] Linde F. and Hvid I. Stiffness behaviour of trabecular bone specimens. *J Biomech*, 20(1):83–89, 1987.

[92] Link T. M., Majumdar S., Augat P., Lin J. C., Newitt D., Lu Y., Lane N. E., and Genant H. K. In vivo high resolution MRI of the calcaneus: differences in trabecular structure in osteoporosis patients. *J Bone Miner Res*, 13(7):1175–1182, 1998.

[93] Lochmüller E. M., Groll O., Kuhn V., and Eckstein F. Mechanical strength of the proximal femur as predicted from geometric and densitometric bone properties at the lower limb versus the distal radius. *Bone*, 30(1):207–216, 2002.

[94] Lochmüller E. M., Miller P., Burklein D., Wehr U., Rambeck W., and Eckstein F. In situ femoral dual-energy x-ray absorptiometry related to ash weight, bone size and density, and its relationship with mechanical failure loads of the proximal femur. *Osteoporos Int*, 11(4):361–367, 2000.

[95] Looker A. C., Orwoll E. S., Johnston Jr., C. C., Lindsay R. L., Wahner H. W., Dunn W. L., Calvo M. S., Harris T. B., and Heyse S. P. Prevalence of low femoral bone density in older U.S. adults from NHANES III. *J Bone Miner Res*, 12(11):1761–1768, 1997.

[96] Lorensen W. E. and Cline H. E. Marching cubes: A high resolution 3d surface contruction algorithm. *Comput Graph*, 21:163–169, 1987.

[97] Lotz J. C., Gerhart T. N., and Hayes W. C. Mechanical properties of trabecular bone from the proximal femur: a quantitative CT study. *J Comput Assist Tomogr*, 14(1):107–114, 1990.

[98] Lu Z. F., Zagzebski J. A., Madsen E. L., and Dong F. A method for estimating an overlying layer correction in quantitative ultrasound imaging. *Ultrason Imaging*, 17:269–290, 1995.

[99] Ludwig G. D. The velocity of sound through tissues and the acoustic impedance of tissues. *J Acoust Soc Am*, 22:862–866, 1950.

[100] Luo G., Kaufman J. J., Chiabrera A., Bianco B., Kinney J. H., Haupt D., Ryaby J. T., and Siffert R. S. Computational methods for ultrasonic bone assessment. *Ultrasound Med Biol*, 25(5):823–830, 1999.

[101] Majumdar S., Kothari M., Augat P., Newitt D. C., Link T. M., Lin J. C., Lang T.,

Lu Y., and Genant H. K. High-resolution magnetic resonance imaging: three-dimensional trabecular bone architecture and biomechanical properties. *Bone*, 22(5):445–454, 1998.

[102] Mele R., Masci G., Ventura V., de Aloysio D., Bicocchi M., and Cadossi R. Three-year longitudinal study with quantitative ultrasound at the hand phalanx in a female population. *Osteoporos Int*, 7(6):550–557, 1997.

[103] Melton 3rd, L. J., Atkinson E. J., O'Fallon W. M., Wahner H. W., and Riggs B. L. Long-term fracture prediction by bone mineral assessed at different skeletal sites. *J Bone Miner Res*, 8(10):1227–1233, 1993.

[104] Morabia A., Ross A., Curtin F., Pichard C., and Slosman D. O. Relation of BMI to a dual-energy x-ray absorptiometry measure of fatness. *Br J Nutr*, 82(1):49–55., 1999.

[105] Neu C. M., Manz F., Rauch F., Merkel A., and Schoenau E. Bone densities and bone size at the distal radius in healthy children and adolescents: a study using peripheral quantitative computed tomography. *Bone*, 28(2):227–232, 2001.

[106] Nicholson P. H. and Bouxsein M. L. Bone marrow influences quantitative ultrasound measurements in human cancellous bone. *Ultrasound Med Biol*, 28(3):369–375, 2002.

[107] Nicholson P. H., Lowet G., Langton C. M., Dequeker J., and Van der Perre G. A comparison of time-domain and frequency-domain approaches to ultrasonic velocity measurement in trabecular bone. *Phys Med Biol*, 41(11):2421–2435, 1996.

[108] Nicholson P. H., Muller R., Cheng X. G., Ruegsegger P., Van Der Perre G., Dequeker J., and Boonen S. Quantitative ultrasound and trabecular architecture in the human calcaneus. *J Bone Miner Res*, 16(10):1886–1892, 2001.

[109] Nicholson P. H. and Strelitzki R. On the prediction of young's modulus in calcaneal cancellous bone by ultrasonic bulk and bar velocity measurements. *Clin Rheumatol*, 18(1):10–16, 1999.

[110] Nicholson P. H., Strelitzki R., Cleveland R. O., and Bouxsein M. L. Scattering of ultrasound in cancellous bone: predictions from a theoretical model. *J Biomech*, 33(4):503–506, 2000.

[111] Nicholson P. H. F., Cheng X. G., Lowet G., Boonen S., Davie M. W. J., Dequeker J., and Van der Perre G. Structural and material mechanical properties of human vertebral cancellous bone. *Med Eng Phys*, 19:729–737, 1997.

[112] Nicholson P. H. F., Haddaway M. J., and Davie M. W. J. The dependence of ultrasonic properties on orientation in human vertebral bone. *Phys Med Biol*, 39(6):1013–1024, 1994.

[113] Njeh C. F., Boivin C. M., and Langton C. M. The role of ultrasound in the assessment of osteoporosis: a review. *Osteoporos Int*, 7(1):7–22, 1997.

[114] Njeh C. F., Fuerst T., Diessel E., and Genant H. K. Is quantitative ultrasound dependent on bone structure? A reflection. *Osteoporos Int*, 12(1):1–15, 2001.

[115] Njeh C. F., Hans D., Fuerst T., Glüer C. C., and Genant H. K. *Quantitative Ultrasound: Assessment of Osteoporosis and Bone Status*. Martin Dunitz Ltd., London, 1999.

[116] Njeh C. F., Hans D., Li J., Fan B., Fuerst T., He Y. Q., Tsuda-Futami E., Lu Y.,

Wu C. Y., and Genant H. K. Comparison of six calcaneal quantitative ultrasound devices: precision and hip fracture discrimination. *Osteoporos Int*, 11(12):1051–1062, 2000.

[117] Njeh C. F., Hodgskinson R., Currey J. D., and Langton C. M. Orthogonal relationships between ultrasonic velocity and material properties of bovine cancellous bone. *Med Eng Phys*, 18(5):373–381, 1996.

[118] Njeh C. F., Kuo C. W., Langton C. M., Atrah H. I., and Boivin C. M. Prediction of human femoral bone strength using ultrasound velocity and BMD: an in vitro study. *Osteoporos Int*, 7(5):471–477, 1997.

[119] Odgaard A. Three-dimensional methods for quantification of cancellous bone architecture. *Bone*, 20(4):315–328, 1997.

[120] Odgaard A. and Gundersen H. J. Quantification of connectivity in cancellous bone, with special emphasis on 3-d reconstructions. *Bone*, 14(2):173–182, 1993.

[121] Odgaard A., Jensen E. B., and Gundersen H. J. Estimation of structural anisotropy based on volume orientation. A new concept. *J Microsc*, 157 (Pt 2):149–162, 1990.

[122] Pacheco E. M., Harrison E. J., Ward K. A., Lunt M., and Adams J. E. Detection of osteoporosis by dual energy x-ray absorptiometry (DXA) of the calcaneus: is the WHO criterion applicable? *Calcif Tissue Int*, 70(6):475–482, 2002.

[123] Parfitt A. M. Trabecular bone architecture in the pathogenesis and prevention of fracture. *Am J Med*, 82(1B):68–72, 1987.

[124] Parfitt A. M., Matthews C. H. E., Villanueva A. R., Kleerekoper M., Frame B., and Rao D. S. Relationships between surface, volume and thickness of iliac trabecular bone in aging and osteoporosis. *J Clin Invest*, 72:1396–1409, 1983.

[125] Paschalis E. P., Shane E., Lyritis G., Skarantavos G., Mendelsohn R., and Boskey A. L. Bone fragility and collagen cross-links. *J Bone Miner Res*, 19(12):2000–2004, 2004.

[126] Patel R., Blake G. M., Herd R. J., and Fogelman I. The effect of weight change on DXA scans in a 2-year trial of etidronate therapy. *Calcif Tissue Int*, 61(5):393–399, 1997.

[127] Patel V., Issever A. S., Burghardt A., Laib A., Ries M., and Majumdar S. MicroCT evaluation of normal and osteoarthritic bone structure in human knee specimens. *J Orthop Res*, 21(1):6–13, 2003.

[128] Phelps M. E., Hoffman E. J., and Ter-Pogossian M. M. Attenuation coefficients of various body tissues, fluids, and lesions at photon energies of 18 to 136 keV. *Radiology*, 117(3 Pt 1):573–583, 1975.

[129] Phillipov G., Seaborn C. J., and Phillips P. J. Reproducibility of DXA: potential impact on serial measurements and misclassification of osteoporosis. *Osteoporos Int*, 12(1):49–54, 2001.

[130] Ragozzino M. Analysis of the error in measurement of ultrasound speed in tissue due to waveform deformation by frequency-dependent attenuation. *Ultrasonics*, 19(3):135–138, 1981.

[131] Rajapakse C. S., Thomsen J. S., Espinoza Ortiz J. S., Wimalawansa S. J., Ebbesen E. N., Mosekilde L., and Gunaratne G. H. An expression relating breaking stress

and density of trabecular bone. *J Biomech*, 37(8):1241–1249, 2004.

[132] Rao P. S. and Gregg E. C. Attenuation of monoenergetic gamma rays in tissues. *Am J Roentgenol Radium Ther Nucl Med*, 123(3):631–637, 1975.

[133] Roberjot V., Bridal S. L., Laugier P., and Berger G. Absolute backscatter coefficient over a wide range of frequencies in a tissue-mimicking phantom containing two populations of scatterers. *IEEE Trans Ultrason Ferroelectr Freq Control*, 43(5):970–978, 1996.

[134] Roux C., Roberjot V., Porcher R., Kolta S., Dougados M., and Laugier P. Ultrasonic backscatter and transmission parameters at the os calcis in postmenopausal osteoporosis. *J Bone Miner Res*, 16(7):1353–1362, 2001.

[135] Ruegsegger P., Koller B., and Muller R. A microtomographic system for the nondestructive evaluation of bone architecture. *Calcif Tissue Int*, 58(1):24–29, 1996.

[136] Sachse W. and Pao Y. H. On the determination of phase and group velocities of dispersive waves in solids. *J Appl Phys*, 49(8):4320–4327, 1978.

[137] Schechter R. S., Chaskelis H. H., Mignogna R. B., and Delsanto P. P. Real-time parallel computation and visualization of ultrasonic pulses in solids. *Science*, 265:1188–1192, 1994.

[138] Serpe L. and Rho J. Y. The nonlinear transition period of broadband ultrasound attenuation as bone density varies. *J Biomech*, 29(7):963–966, 1996.

[139] Seung H., Medige J., and Ziv I. Combined models of ultrasound velocity and attenuation for predicting trabecular bone strength and mineral density. *Clin Biomech*, 11(6):348–353, 1996.

[140] Sievänen H., Oja P., and Vuori I. Precision of dual-energy x-ray absorptiometry in determining bone mineral density and content of various skeletal sites. *J Nucl Med*, 33(6):1137–1142, 1992.

[141] Silva M. J. and Gibson L. J. Modeling the mechanical behavior of vertebral trabecular bone: effects of age-related changes in microstructure. *Bone*, 21(2):191–199, 1997.

[142] Sokal R. R. *Biometry: the principles and practice of statistics in biological research.* Freeman, San Francisco, 1981.

[143] Sorenson J. A. Effects of nonmineral tissues on measurement of bone mineral content by dual-photon absorptiometry. *Med Phys*, 17(5):905–912, 1990.

[144] Spotila L. D., Constantinou C. D., Sereda L., Ganguly A., Riggs B. L., and Prockop D. J. Mutation in a gene for type i procollagen (COL1A2) in a woman with postmenopausal osteoporosis: evidence for phenotypic and genotypic overlap with mild osteogenesis imperfecta. *Proc Natl Acad Sci U S A*, 88(12):5423–5427, 1991.

[145] Stegman M. R., Heaney R. P., and Recker R. R. Comparison of speed of sound ultrasound with single photon absorptiometry for determining fracture odds ratios. *J Bone Miner Res*, 10(3):346–352, 1995.

[146] Stevens A. and Lowe J. *Human histology.* Mosby, London, 2nd edition edition, 1997.

[147] Stewart A., Torgerson D. J., and Reid D. M. Prediction of fractures in perimenopausal women: a comparison of dual energy x ray absorptiometry and broad-

band ultrasound attenuation. *Ann Rheum Dis*, 55(2):140–142, 1996.

[148] Svendsen O. L., Hassager C., Skodt V., and Christiansen C. Impact of soft tissue on in vivo accuracy of bone mineral measurements in the spine, hip, and forearm: a human cadaver study. *J Bone Miner Res*, 10(6):868–873, 1995.

[149] Swanpalmer J. and Kullenberg R. A new measuring device for quantifying the amount of mineral in the heel bone. *Ann N Y Acad Sci*, 904:115–117, 2000.

[150] Theisman H. and Pfander F. Uber die durchlässigkeit des knochens fur ultraschall. *Strahlentherapie*, 80:607–610, 1949.

[151] Thompson P., Taylor J., Fisher A., and Oliver R. Quantitative heel ultrasound in 3180 women between 45 and 75 years of age: compliance, normal ranges and relationship to fracture history. *Osteoporos Int*, 8(3):211–214, 1998.

[152] Tothill P., Hannan W. J., Cowen S., and Freeman C. P. Anomalies in the measurement of changes in total-body bone mineral by dual-energy x-ray absorptiometry during weight change. *J Bone Miner Res*, 12(11):1908–1921, 1997.

[153] Tothill P. and Pye D. W. Errors due to non-uniform distribution of fat in dual x-ray absorptiometry of the lumbar spine. *Br J Radiol*, 65(777):807–813, 1992.

[154] Townsend P. R., Raux P., Rose R. M., Miegel R. E., and Radin E. L. The distribution and anisotropy of the stiffness of cancellous bone in the human patella. *J Biomech*, 8(6):363–367, 1975.

[155] Turner C. H. Yield behavior of bovine cancellous bone. *J Biomech Eng*, 111(3):256–260, 1989.

[156] Turner C.H. and Burr D.B. Basic biomechanical measurements of bone: a tutorial. *Bone*, 14(4):595–606, 1993.

[157] Töyräs J., Kröger H., and Jurvelin J. S. Bone properties as estimated by mineral density, ultrasound attenuation, and velocity. *Bone*, 25(6):725–731, 1999.

[158] Töyräs J., Nieminen M. T., Kröger H., and Jurvelin J. S. Bone mineral density, ultrasound velocity, and broadband attenuation predict mechanical properties of trabecular bone differently. *Bone*, 31(4):503–507, 2002.

[159] Urick R. J. A sound velocity method for determining the compressibility of finely divided substances. *J Appl Phys*, 18:983–987, 1947.

[160] Vahey J. W., Lewis J. L., and Vanderby Jr., R. Elastic moduli, yield stress, and ultimate stress of cancellous bone in the canine proximal femur. *J Biomech*, 20(1):29–33, 1987.

[161] Van Rietbergen B., Huiskes R., Eckstein F., and Ruegsegger P. Trabecular bone tissue strains in the healthy and osteoporotic human femur. *J Bone Miner Res*, 18(10):1781–1788, 2003.

[162] Waarsing J. H., Day J. S., and Weinans H. An improved segmentation method for in vivo microCT imaging. *J Bone Miner Res*, 19(10):1640–1650, 2004.

[163] Wachter N. J., Augat P., Mentzel M., Sarkar M. R., Krischak G. D., Kinzl L., and Claes L. E. Predictive value of bone mineral density and morphology determined by peripheral quantitative computed tomography for cancellous bone strength of the proximal femur. *Bone*, 28:133–139, 2001.

[164] Wallach S., Feinblatt J. D., Carstens J. H. Jr., and Avioli L. V. The bone "quality"

problem. *Calcif Tissue Int*, 51(3):169–172, 1992.

[165] Wang X., Bank R. A., TeKoppele J. M., and Agrawal C. M. The role of collagen in determining bone mechanical properties. *J Orthop Res*, 19:1021–1026, 2001.

[166] Wear K. A. Frequency dependence of ultrasonic backscatter from human trabecular bone: theory and experiment. *J Acoust Soc Am*, 106(6):3659–3664, 1999.

[167] Wear K. A. Anisotropy of ultrasonic backscatter and attenuation from human calcaneus: implications for relative roles of absorption and scattering in determining attenuation. *J Acoust Soc Am*, 107(6):3474–3479, 2000.

[168] Wear K. A. The effects of frequency-dependent attenuation and dispersion on sound speed measurements: Applications in human trabecular bone. *IEEE Trans Ultrason Ferroelectr Freq Control*, 47(1):265–273, 2000.

[169] Wear K. A. Measurement of dependence of backscatter coefficient from cylinders on frequency and diameter using focused transducers–with applications in trabecular bone. *J Acoust Soc Am*, 115(1):66–72, 2004.

[170] Wear K. A. and Armstrong D. W. Relationships among calcaneal backscatter, attenuation, sound speed, hip bone mineral density, and age in normal adult women. *J Acoust Soc Am*, 110(1):573–578, 2001.

[171] Wear K. A. and Garra B. S. Assessment of bone density using ultrasonic backscatter. *Ultrasound Med Biol*, 24(5):689–695, 1998.

[172] Wear K. A., Stuber A. P., and Reynolds J. C. Relationships of ultrasonic backscatter with ultrasonic attenuation, sound speed and bone mineral density in human calcaneus. *Ultrasound Med Biol*, 26(8):1311–1316, 2000.

[173] Wells P. N. T. *Physical Principles of Ultrasonic Diagnosis.* Academic Press, London, 1969.

[174] Wells P. N. T. *Biomedical Ultrasonics.* Academic Press, London, 1977.

[175] Wolff J. *Das Gesetz der Transformation der Knochen.* Hirchwild, Berlin, 1892.

[176] Wood A. B. *Textbook of Sound.* G. Bell and Sons Ltd., London, 1932.

[177] World Healt Organization. Assessment of fracture risk and its application to screening for postmenopausal osteoporosis. Technical Report series 843, WHO, 1994.

[178] Wu C. Y., Glüer C. C., Jergas M., Bendavid E., and Genant H. K. The impact of bone size on broadband ultrasound attenuation. *Bone*, 16(1):137–141, 1995.

[179] Yao X.L., Zagzebski J.A., and Madsen E.L. Backscatter coefficient measurements using a reference phantom to extract depth dependent instrumentation factors. *Ultrason Imaging*, 12:58–70, 1990.

[180] Zysset P. K. A review of morphology-elasticity relationships in human trabecular bone: theories and experiments. *J Biomech*, 36(10):1469–1485, 2003.

Kuopio University Publications C. Natural and Environmental Sciences

C 178. Riikonen, Johanna. Modification of the growth, photosynthesis and leaf structure of silver birch by elevated CO2 and O3.
2004. 126 p. Acad. Diss.

C 179. Frank, Christian. Functional profiling of the xenobiotic nuclear receptors CAR and PXR.
2004. 87 p. Acad. Diss.

C 180. Rytkönen, Esko. High-frequency vibration and noise in dentistry.
2005. 80 p. Acad. Diss.

C 181. Seppänen, Aku. State estimation in process tomography.
2005. 117 p. Acad. Diss.

C 182. Ibrahim, Mohamed Ahmed. Plant essential oils as plant protectants and growth activators.
2005. 143 p. Acad. Diss.

C 183. Vuorinen, Terhi. Induced volatile emissions of plants under elevated carbon dioxide and ozone concentrations, and impacts on indirect antiherbivore defence.
2005. 98 p. Acad. Diss.

C 184. Savinainen, Juha. Optimized methods to determine ligand activities at the cannabinoid CB1 and CB2 receptors.
2005. 83 p. Acad. Diss.

C 185. Luomala, Eeva-Maria. Photosynthesis, chemical composition and anatomy of Scots pine and Norway spruce needles under elevated atmospheric CO2 concentration and temperature.
2005. 137 p. Acad. Diss.

C 186. Heikkinen, Lasse M. Statistical estimation methods for electrical pricess tomography.
2005. 147 p. Acad. Diss.

C 187. Riihinen, Kaisu. Phenolic compounds in berries.
2005. 97 p. Acad. Diss.

C 188. Virkutyte, Jurate. Heavy metal bonding and remediation conditions in electrokinetically treated waste medias.
2005. 133 p. Acad. Diss.

C 189. Koistinen, Kaisa. Birch PR-10c: multifunctional binding protein.
2006. 79 p. Acad. Diss.

C 190. Airaksinen, Sanna. Bedding and manure management in horse stables: its effect on stable air quality, paddock hygiene and the compostability and utilization of manure.
2006. 91 p. Acad. Diss.

C 191. Asikainen, Arja. Use of computational tools for rapid sorting and prioritising of organic compounds causing environmental risk with estrogenic and cytochrome P450 activity.
2006. 51 p. Acad. Diss.

C 192. Ålander, Timo. Carbon composition and volatility characteristics of the aerosol particles formed in internal combustion engines.
2006. 54 p. Acad. Diss.